Insight into the adsorption kinetics models for the removal of contaminants from aqueous solutions

K.L. Tan, B.H. Hameed*

School of Chemical Engineering, Engineering Campus, Universiti Sains Malaysia, 14300 Nibong Tebal, Penang, Malaysia

ARTICLE INFO

ABSTRACT

The past decade has seen a boom in environmental adsorption studies on the adsorptive removal of pollutants from the aqueous phase. A large majority of works treat kinetic modeling as a mere routine to describe the macroscopic trend of adsorptive uptake by using common models, often without careful appraisal of the characteristics and validity of the models. This review compiles common kinetic models and discusses their origins, features, modified versions (if any), and applicability with regard to liquid adsorption modeling for both batch adsorption and dynamic adsorption systems. Indiscriminate applications, ambiguities, and controversies are highlighted and clarified. The appropriateness of linear regression for correlating kinetic data is discussed. This review concludes with a note on the current scenario and the future of kinetics modeling of liquid adsorption.

1. Introduction

Adsorption is one of the most widely used technologies for removing pollutants from contaminated aqueous media. It is preferred over other methods because of its relatively simple design, operation, cost effectiveness, and energy efficiency [1]. The importance of adsorption for water and wastewater treatment is growing in view of the presence of emerging contaminants, such as pharmaceuticals and personal care products (PPCPs), in water bodies [2,3].

Water pollutants in the environmental adsorption literature can be generally categorized into six groups: (i) heavy metals, (ii) phenolics, (iii) dyes, (iv) pesticides, (v) PPCPs, and (vi) others (hydrocarbons, inorganic anions, etc.). These pollutants are found dissolved in water and wastewater in various concentrations. Numerous solid adsorbents with wide-ranging characteristics have been developed for removing these dissolved pollutants [4–9]. Basic classes of adsorbents include activated carbon, zeolite, clay, mesoporous silica, polymeric resin, and metal-organic frameworks.

The design and scale-up of an adsorption system require knowledge of adsorption equilibrium and kinetics. The development of kinetics understanding is largely limited by the theoretical complexity of adsorption mechanisms. Many models of varied complexity have been developed to predict the uptake rate of the adsorptive into the adsorbent [10,11]. Pseudo-first-order (PFO) and pseudo-second-order (PSO) models are the two most commonly used empirical models in liquid adsorption studies.

Most works focus on the novelty of the material. The kinetics studies in these works, in which experimental data are fitted to PFO and PSO models, serve merely to complement the adsorbent evaluation. Strong knowledge of the origins, strengths, and limitations of these models is sorely missing, as evident from these works. Little effort is made to investigate the underlying physico-chemical phenomena after the model fitting is completed. As such, the model parameters are merely empirical constants that have no distinct theoretical significance. Several works have attempted to rationalize these two empirical models and find the theoretical differences between them [12–15].

Ho [16] reviewed the applications of second-order models to adsorption systems. Liu and Liu [17] summarized the useful kinetic models for biosorption. Plazinski et al. [16] reviewed the adsorption kinetic models that had been theoretically associated with surface reaction mechanism. Batch and dynamic adsorption models were discussed by Alberti et al. [10]. However, these reviews were limited to selected models, and the discussion may have been overly complex for general or beginner readers. This review adopts a more general approach to reporting the major studies. It aims for a wider audience while retaining the essence of the kinetic studies.

The objective of this review is to promote better understanding of the kinetic modeling of liquid adsorption systems. While the focus is on batch adsorption, continuous fixed bed adsorption is discussed as well. Kinetic models relevant to aqueous adsorption

* Corresponding author.
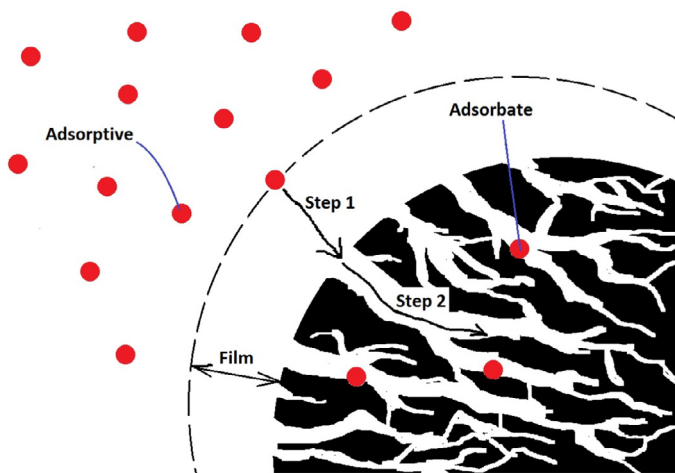E-mail address: chbassim@usm.my (B.H. Hameed).

Fig. 1. Adsorption of an adsorptive molecule onto the internal surface of a porous adsorbent pellet. Step 1 is film diffusion, and Step 2 is pore diffusion.

kinetics in environmental remediation are presented. This paper also attempts to clarify ambiguities and doubts with regard to these models. The features and applicability of the models are discussed with reference to the literature. Theoretical origins or interpretations and modified versions of models are discussed where applicable.

The second objective is to highlight concerns in model discrimination. Issues arising from the selection of linear or nonlinear regression are brought to light. Certain widely used statistical error functions for regression and model comparison purposes are presented. This paper concludes with a summary of the modeling scenes of liquid adsorption kinetics, along with comments on the future of the field from the authors' perspective.

2. Principles of adsorption process

Adsorption is a surface phenomenon in which adsorptive (gas or liquid) molecules bind to a solid surface. However, in practice, adsorption is performed as an operation, either in batch or continuous mode, in a column packed with porous sorbents. Under such circumstances, mass transfer effects are inevitable. The complete course of adsorption includes mass transfer and comprises three steps [18]:

Step 1: Film diffusion (external diffusion), which is the transport of adsorptive from the bulk phase to the external surface of adsorbent.

Step 2: Pore diffusion [intraparticle diffusion (IPD)], which is the transport of adsorptive from the external surface into the pores.

Step 3: Surface reaction, which is the attachment of adsorptive to the internal surface of sorbent.

Fig. 1 depicts the trajectory of an adsorptive molecule during adsorption. The first two steps are transport steps, and the last step is a reaction step (Step 3, not labeled in Fig. 1). Each step presents a resistance to the adsorptive. The overall adsorption rate (as measured through an experiment) is determined by total resistance, which is the sum of the three component resistances in series [19]. The reduction of any component resistance increases the adsorption rate. The third step is typically very rapid compared with the first and second steps, and therefore poses negligible resistance. If one step contributes dominantly to the total resistance, to the point that reducing the other two resistances only marginally increases the adsorptive uptake rate, then the step is called a sole

rate-controlling step. The transport resistances depend on numerous factors, including adsorbent and adsorptive types, their properties, and operating conditions. The rate-controlling step can change during the adsorption process [20]. For dye adsorption on pine sawdust, the controlling mechanism switches from surface reaction to IPD when the adsorbent is 80% saturated [21].

Two types of interaction, namely, physical and chemical, are possible between adsorbent and adsorbate [22,23]; the former is known as physisorption, and the latter is chemisorption. Physisorption is a result of attractive forces between sorbent and adsorbate molecules [24], whereas chemisorption provides a stronger bond as it involves the transfer or sharing of electrons between adsorbent and adsorbate species. As a guideline, an isosteric heat of adsorption with magnitude between 5 and 40 kJ/mol indicates physisorption as the dominant adsorption mode, while one between 40 and 125 kJ/mol indicates chemisorption [25,26].

The monolayer capacity of an adsorbent is its capacity to accommodate a single layer of adsorbed species on the adsorbent surface. Often, when adsorptive concentration is high, because of intermolecular attraction, additional layers stack onto the first monolayer, thereby forming multilayer adsorption, which is physical in nature [22].

The heterogeneity of the adsorbent surface significantly affects adsorption equilibrium and kinetics. Heterogeneous adsorbents contain more than one type of adsorption site that can bind the adsorbate, and each site type has a different heat of adsorption. Surprisingly, Langmuir isotherm, which is based on homogeneous surface sites, can describe a large number of adsorption systems, many of which possess heterogeneous surface characteristics [27].

Adsorption study comprises two main aspects: equilibrium and kinetic studies. The attainment of equilibrium in adsorptive loading by the adsorbent is governed by thermodynamics. The rate of adsorptive uptake is dependent on the adsorption mechanism. The understanding of adsorption equilibrium has matured, as a wide variety of equilibrium isotherms exist for describing the equilibrium uptake of any target adsorptive. Conversely, adsorption kinetics theory is developing far more slowly despite its importance to practical applications of a given sorbent. The basis for kinetics study is the kinetic isotherm, which is obtained experimentally by tracking the adsorbed amount against time. Kinetic investigations develop a model to describe the adsorption rate. Ideally, the model should, with minimal complexity, (i) reveal the rate-limiting mechanism and (ii) extrapolate to operating conditions of interest. Accomplishing these two targets should enable one to identify operating conditions with minimal mass transfer resistance and predict adsorbent performance.

3. Modeling the kinetics of batch adsorption

3.1. Kinetic experiment

Adsorption kinetics can be represented by a plot of uptake vs. time; this plot is known as a kinetic isotherm. This plot forms the basis of all kinetics studies because its shape represents the underlying kinetics of the process. The kinetics are dependent on material factors, such as adsorbent and adsorbate types, and experimental factors, such as temperature and pH [28,29]. Typically, a batch experiment is conducted to collect kinetic data. Ensuring constant experimental conditions during batch adsorption is important.

The kinetic isotherm should ideally shed light on the intrinsic kinetics, which are the chemical kinetics on the adsorbent surface in the absence of transport limitations. Batch operation is an attractive method for studying intrinsic kinetics. Mass transfer effects are relatively easily reduced or eliminated by applying (i) high agitation speed (reduced film thickness) and (ii) small particle size (reduced pore diffusion resistance) [30].

The adsorptive uptake per unit mass of adsorbent, q (mg/g) is

$$q = \frac{(C_0 - C)V}{m} \tag{1}$$

where C_0=initial concentration of adsorptive in the bulk liquid (mg/l); C_0=concentration of adsorptive in the bulk liquid at time t (mg/l); V=volume of the bulk solution (l); m=mass of adsorbent (g)

3.2. Adsorption–reaction model

3.2.1. Pseudo-first-order (PFO) equation and pseudo-second-order (PSO) equation

3.2.1.1. Pseudo-first-order equation. The pseudo-first-order (PFO) equation was proposed by Largergren in 1898 for adsorption of oxalic and malonic acid onto charcoal [31]. It has the following differential form:

$$\frac{dq}{dt} = k_1(q_e - q) \tag{2}$$

where q=adsorption capacity (mg/g); t=time(min) and k_1 = rate constant (1/min). Upon integrating with the initial conditions of $q = 0$ when $t = 0$, Eq. (2) yields

$$q = q_e(1 - \exp(-kt)) \tag{3}$$

Its linearized form is

$$\ln(q_e/(q_e - q)) = k_1 t \tag{4}$$

Plotting $\ln((q_e - q)/q_e)$ vs. t gives a straight line that passes through the origin with a slope k_1 for systems that obey this model.

The rate constant k_1 is a function of the process conditions. It is reported to decrease with increasing initial bulk concentration [32–35], which may be understood as follows: $1/k_1$ is the time scale for the process to reach equilibrium; a longer time is needed (smaller k_1) if the initial concentration (C_0) is larger. Some reports have found that k_1 is an increasing function of C_0 or independent of C_0 [36,37]. k_1 value is expected to be influenced by experimental conditions, such as pH and temperature. As equilibrium behavior (isotherms) is affected by these two factors, isolating their effects to k_1 value would be experimentally difficult. As expected, small particle size is associated with large values of k_1 [38].

The PFO model has been argued to be valid for long adsorption times when the system is near equilibrium [11,39]. The model has also been shown to be valid only at the initial stage of adsorption [40,41]. No generalization can be drawn from this apparent contradiction because systematic comparisons are made impossible by the high variability of experimental conditions, such as concentration range and adsorbent dosage. No consensus has been reached on "standard" operating conditions; as such, a wide array of data are reported from which no meaningful comparisons or conclusions with regard to kinetics can be drawn [17,42,43]. An example of this situation is in parametric studies (where the effects of the operating parameters are studied), in which only the range of the variable parameter under study is reported, whereas the accompanying set of constant conditions is not completely stated.

The rate-controlling mechanism depends on the experimental conditions and surface coverage (adsorption time). Consequently, the validity of a model is limited to a certain operating range of the assumed mechanism under which it is developed or interpreted. Douven et al. [44] defined three dimensionless numbers that define the range of validity of three kinetic models. Pseudo-first-order models are valid only under either of these two sets of conditions: (i) reaction control and Henry regime adsorption, or (ii) reaction control and high adsorbent dose. A modified PFO was presented [45]

$$\frac{dq}{dt} = k_1 \frac{q_e}{q}(q_e - q) \tag{5}$$

with the linearized form

$$\frac{q}{q_e} + ln(q_e - q) = \ln(q_e) - k_1 t \tag{6}$$

This modified form considers a variable rate constant $k_1 q_e / q$ and outperforms PFO and PSO in monitoring the adsorption kinetics of dyes on activated carbon [45]. Theoretical derivations of this modified PFO model have been given by Azizian and Bashiri [46] and Rudzinski and Plazinski [47].

3.2.1.2. Pseudo-second-order model
This model assumes that the uptake rate is second order with respect to the available surface sites [48].

$$\frac{dq}{dt} = k_2(q_e - q)^2 \tag{7}$$

where k_2 is the pseudo-second-order (PSO) rate constant. Other symbols have the same meanings as in the PFO model. Integrating Eq. (7) with initial conditions of $q = 0$ when $t = 0$ and subsequent rearrangement obtains the linearized form.

$$\frac{t}{q} = \frac{1}{k_2 q_e^2} + \frac{t}{q_e} \tag{8}$$

The initial rate of adsorption ($q(t \to 0)$) is $k_2 q_e^2$. A plot of $\frac{t}{q}$ vs t gives a straight line for PSO-compliant kinetics. The slope is $\frac{1}{q_e}$, and the intercept is $\frac{1}{k_2 q_e^2}$. Other linearized forms are available but less frequently used [49].

Most environmental kinetic adsorption can be modeled well by PSO, thereby indicating its superiority to other models. Similar to PFO's k_1, the constant k_2 is a time scale factor that decreases with increasing C_0 [50–53]. The effects of pH and temperature on k_2 are not well studied because of difficulties that arise from the effects on equilibrium isotherm shapes. Small particle size yields a larger k_2 value because of reduced IPD resistance [38].

Douven et al. [44] proposed an adsorption–diffusion model based on pore diffusion and Langmuir surface reaction. Their model provides an excellent fit to PSO kinetics if the following conditions are fulfilled: (i) reaction control, nonlinear (saturated) adsorption, and (ii) a sufficient amount of adsorbent to adsorb half of the adsorptive in the bulk phase. They argued that those PSO kinetics that cannot be modeled by their model are controlled by an unknown mechanism, at least over a certain time range.

3.2.1.3. Remarks on pseudo-first-order equation and pseudo-second-order equation. The PFO and PSO models are the most popular models in environmental adsorption kinetics studies. However, in most cases, PFO is inferior in terms of fit to the pseudo-second-order model by a least-square discrimination procedure; its q_e is often much farther from the experimental value compared with that given by the pseudo-second-order model [54–56].

Plazinski et al. [11] showed that PSO's wide applicability over PFO does not necessarily stem from a physical basis, but a mathematical basis. During PSO model linearization, the random errors in measured q_e values are not altered as heavily as in the case of PFO. The calculated q_e is often less than, but close to, the experimental value. An advantage of applying PSO is that equilibrium q_e value is not required for data fitting. However, experimental q_e does provide a check on the calculated q_e and is therefore advised.

Numerous environmental adsorption studies fit the PFO and PSO models to the same set of kinetic data. Better fits are determined using the statistical least squares method. Under controlled reactions, the rate constants (k_1 and k_2, respectively, for PFO and PSO) are regarded as reaction rate constants. However, in most adsorption studies, the adsorption is generally assumed to be performed in a reaction-controlled regime, without explicit reports on whether any effort has been made to reduce/eliminate

the transport influences. The fitted rate constants k_1 and k_2 are most probably lumped constants that combine reaction and diffusion effects under specific experimental conditions. These lumped constants are merely empirical constants without physicochemical significance, as they cannot relate to the underlying adsorption mechanisms [57]. Kinetic studies of this type are largely a data correlation exercise that, on the one hand, provides little insight into the controlling mechanisms and, on the other hand, complicates further analysis (if any) for design and scaling purposes.

The mixed reaction diffusion rate constant is complex to resolve for complete elucidation of the intrinsic kinetics [58]. If the obtained rate constant is a reaction rate constant (rather than a mixed reaction–diffusion constant), then the Arrhenius equation can be applied meaningfully to calculate its adsorption activation energy [59,60]. For column design, studying the diffusion-controlled kinetics and reaction-controlled kinetics in separate experiments rather than single experiments is advisable [61–63].

The PFO and PSO models lack theoretical basis as they are not derived based on a pre-assumed reaction mechanism. They remained largely empirical until 2004, when Azizian proposed his interpretation of these topical models based on Langmuir surface kinetics [64]. According to his theoretical interpretation, which is supported by other studies, PFO fits better when C_0 is high, while PSO fits better when C_0 is not excessively high. As high concentration is not definitive, exceptions are common [65–67].

Although PFO and PSO models are associated with surface reaction control systems [12,13,68], Rudzinski and Plazinski [39] illustrated mathematically that PFO fit can be an indication of IPD and/or surface reaction-controlled kinetics. Plazinski [69] later found that PFO could be derived by assuming film diffusion control and/or surface reaction control processes. k_1 has different physical meanings under these different regimes. Under his model, k_1 is invariant with initial bulk concentration in the case of film diffusion-controlled kinetics.

Plazinski et al. [70] found that the PSO model can simulate the behavior of an IPD model. Under such transport control, k_2 value should be assumed as a transport rate constant. However, as mentioned above, PSO, like PFO, has long been assumed to be a representation of surface reaction-controlled kinetics, where k_2 is the reaction rate constant.

The aforementioned interpretations apparently indicate that PFO and PSO are not a model of defined mechanism but, rather, a highly flexible formula that combines many different models with different controlling mechanisms. This concept is especially true for PSO, which demonstrates good fitting over the whole time range for almost all liquid adsorption systems. Over a wide range of agitation speeds, which correspond to cases of reduced film diffusion resistance, PSO correlates the broad spectrum of kinetic data equally well [54,71,72]. This finding shows that PSO is merely a general formula with a k_2 value that is a result of complex interplay between different controlling mechanisms. Exploiting the empirical nature of PSO, Azizian and Fallah [73] proposed modified PSO models for improved data fit.

In short, efforts to determine the rate-controlling mechanism based on PFO or PSO curve fit are essentially futile, as multiple conclusions are possible according to the existing theories of these two models. A better approach would be careful control of experimental conditions to effect an appropriately controlled regime, which would obtain semi-empirical, albeit more meaningful, k_1 or k_2 values.

Despite the availability of alternative models, PSO and PFO remain the most popular model for batch processes. All kinetic phenomena are lumped into the rate constant k in an obscure manner. No meaningful mechanism can be confidently postulated from these models. However, for either batch or continuous system design, a lumped analysis is sufficient [74–77]. As these empirical models are more descriptive than predictive, the kinetic experiments for design purpose should be conducted under conditions as close as possible to the target large-scale operation. The practical significance, high curve-fitting capability, and easy manipulation of these lumped kinetic models may explain their continuing widespread acceptance in the modeling of liquid adsorption kinetics.

3.2.2. Elovich equation

First proposed by Roginsky and Zeldovich in 1934 to describe the adsorption of CO on manganese dioxide, the Elovich equation is expressed as [78]

$$\frac{dq}{dt} = \alpha \, \exp(-\beta q) \tag{9}$$

The integrated form is

$$q = \frac{1}{\beta} ln(1 + \alpha\beta t) \tag{10}$$

The more frequently used form is based on the assumption $\alpha\beta t >> 1$. The linearized form is

$$q = \frac{1}{\beta} ln(\alpha\beta) + \frac{1}{\beta} \ln t \tag{11}$$

Kinetics observing the Elovich equation should produce a straight line on the plot of q vs. $\ln t$. The slope is $1/\beta$, and the intercept is $[\ln(\alpha\beta)]/\beta$. α is the initial adsorption rate (mg/g·min), and β is a desorption constant related to the extent of surface coverage and activation energy for chemisorption.

The Elovich equation neglects desorption and is known to describe chemisorption well [79]. It is physically unsound as it predicts infinite q at long periods of time. Therefore, it is suitable for kinetics far from equilibrium where desorption does not occur because of low surface coverage.

Many works have attempted to establish a theoretical basis for the Elovich equation [80–82], and most of these works assume strong heterogeneity at the adsorbent surface.

This model has found applications in liquid phase kinetics modeling. Largitte and Pasquier [83] found Elovich equation to be the best fit for lead adsorption onto activated carbon. Elkady et al. [84] discovered that dye adsorption on eggshell biocomposite beads followed Elovich kinetics. As expected from their physical meanings, the constants α and β increase with increasing initial dye concentration. When the bulk solution temperature increased, observed values of α increased, but β decreased [85].

3.2.3. First-order reversible reaction model

The surface reaction can be considered a first-order reversible reaction [34]

$$A \leftrightarrow B \tag{12}$$

with adsorption rate constant k_a and desorption rate constant k_d. Starting from the rate equation,

$$\frac{dC_B}{dt} = -\frac{dC_A}{dt} = k_a C_A - k_d C_B \tag{13}$$

we can arrive at the final form

$$ln\left(1 - \frac{C_{A0} - C_A}{C_{A0} - C_e}\right) = -(k_a + k_d)t \tag{14}$$

where C_{A0} = initial bulk concentration of adsorptive (mg/l)

C_A = concentration of adsorptive in bulk solution at time t (mg/l)

C_e = equilibrium concentration of adsorptive (mg/l)

To calculate k_a and k_d, two simultaneous equations are needed: Eq. (13) and the equilibrium relation

$$\frac{k_a}{k_d} = \frac{C_{Be}}{C_{Ae}}. \tag{15}$$

This ratio is a constant that is analogous to the Henry constant in the Langmuir isotherm. This is the limiting form for Langmuir kinetics model when adsorption is in the Henry regime. In the Langmuir kinetics model, maximum adsorbable species A is bounded by the monolayer capacity. However, in a first-order reversible reaction model, such saturation effects are not considered in the reaction scheme given by Eq. (12).

This form closely resembles the PFO equation. In practice, differences between their fitting suitability are insignificant [86–88].

3.2.4. Avrami equation

The adsorption rate coefficient might have a temporal dependency during the adsorption process [89]. A kinetic system with a time-dependent rate coefficient is said to exhibit "fractal-like kinetics." The Avrami rate equation is one model that describes such kinetic behavior [90,91]. The equation is

$$\frac{dq}{dt} = k \cdot n \cdot t^{n-1}(q_e - q) \tag{16}$$

where k is the Avrami kinetic constant, and n is a model constant related to the adsorption mechanism. $k_n t^{n-1}$ can be construed as the effective rate coefficient. The integral form is (for $q(t=0)=0$)

$$q = q_e - q_e \exp(-kt^n) \tag{17}$$

This rate equation is first order with respect to the driving force (q_e-q) but can be of fractional order with respect to t, as n can be an integer or fraction. For $n=1$, a PFO results.

The uptake of Cu(II), Mn(II), and Pb(II) was excellently correlated by this Avrami rate equation by using nonlinear regression [92].

The linearized form is

$$ln\left(ln\frac{q_e}{q_e - q}\right) = n \cdot ln\ k + n \cdot ln\ t \tag{18}$$

The values of n and k can be obtained from the slope and intercept, respectively, from a plot of $ln(ln\frac{q_e}{q_e-q})$vs. $ln\ t$. For the adsorption of mercury on chitosan membranes, two straight lines are found on this plot, giving two n values and two k values for the mercury adsorption process [91].

Models that describe kinetics of fractional orders are lacking. The general order model was developed to compensate for the deficiencies of PFO and PSO, which has preset integral reaction orders [93,94]. In the general order model, the reaction order n can be an integer or non-integer rational number, and must be determined by an experiment. The general order model reads

$$\frac{dq}{dt} = k_n(q_e - q)^n \tag{19}$$

with the integrated form

$$q = q_e - \frac{q_e}{\left(k_n q_e^{n-1}t(n-1) + 1\right)^{\frac{1}{n-1}}}; n \neq 1 \tag{20}$$

In two recent studies, the general order model with fractional order best describes the adsorption of pharmaceuticals [95] and synthetic dye onto activated carbon [96].

The Avrami model and general order model can be combined into a general equation form [97,98]

$$\frac{dq}{dt} = k_n t^{m-1}(q_e - q)^n \tag{21}$$

The integrated expression is

$$q = q_e - \frac{1}{\left(\frac{k_n(n-1)t^m}{m} + \frac{1}{q_e^{n-1}}\right)^{\frac{1}{n-1}}}; n \neq 1 \tag{22}$$

The subscript n in k_n denotes the reaction order with respect to the driving force. For $n=1$, Eq. (21) reduces to the Avrami Eq. (16); for $m=1$, Eqs. (21) and (22) reduce to Eqs. (19) and (20), respectively.

3.3. Adsorption–diffusion model

3.3.1. Crank model

A typical model that considers IPD is Fick's second law [99]

$$\frac{\partial q}{\partial t} = \frac{D}{r^2}\frac{\partial}{\partial r}\left(r^2\frac{\partial q}{\partial r}\right) \tag{23}$$

Eq. (23) describes the diffusion of adsorptive in a spherical particle. Symbols D and r respectively denote the intraparticle diffusivity (cm²/min) and the radial distance (cm) from the center of the particle. External diffusion and surface reaction are assumed to be more rapid than IPD. In this equation, the adsorbed amount q is a function of t and r, i.e., $q=f(r,t)$.

Assuming that q at the particle's external surface is constant (i.e., infinite volume of bulk solution) and the particle is initially free of adsorbate, Crank presented an analytical solution for Eq. (23) [100]:

$$\frac{q}{q_e} = 1 + \frac{2R}{\pi r}\sum_{n=1}^{\infty}\frac{(-1)^n}{n}sin\frac{n\pi r}{R}exp\left(\frac{-Dn^2\pi^2 t}{R^2}\right) \tag{24}$$

The average value of q in the spherical particle of radius R at any particular time is $\bar{q}$, calculated as

$$\bar{q} = \frac{3}{R^3}\int_0^R qr^2 dr \tag{25}$$

Substituting Eq. (24) into Eq. (25) and integrating

$$\frac{\bar{q}}{q_e} = 1 - \frac{6}{\pi^2}\sum_{n=1}^{\infty}\frac{1}{n^2}exp\left(-\frac{Dn^2\pi^2 t}{R^2}\right) \tag{26}$$

The bulk-phase adsorptive concentration is

$$C = C_0 - \frac{m}{V}\bar{q} \tag{27}$$

For a short time $\frac{\bar{q}}{q_e} < 0.3$, Eq (26) can be simplified as

$$\frac{\bar{q}}{q_e} = 6\sqrt{\left(\frac{Dt}{\pi R^2}\right)} \tag{28}$$

The diffusion coefficient D for a short time can be determined from a plot of $\frac{\bar{q}}{q_e}$ vs. $\sqrt{t}$. The long time behavior $\frac{\bar{q}}{q_e} > 0.85$ for Eq. (26) is exponential [83], as given by Eq. (29)

$$\frac{\bar{q}}{q_e} = 1 - \frac{6}{\pi^2}exp\left(-\frac{D\pi^2 t}{R^2}\right) \tag{29}$$

Eq. (29) is sometimes called Boyd equation [101,102].

3.3.2. Vermeulen model

Vermeulen proposed an approximate solution to Eq. (26) that is valid over the entire time range [103,104].

$$\frac{\bar{q}}{q_e} = \sqrt{1 - exp\left(-\frac{D\pi^2 t}{R^2}\right)} \tag{30}$$

In the linearized form,

$$ln\left(1 - \left(\frac{\bar{q}}{q_e}\right)^2\right) = -\frac{D\pi^2 t}{R^2} \tag{31}$$

Eq. (31) has been given different names in the literature. It is also known as Dumwald–Wagner model [105–107] or pore-surface mass diffusion model [108–110]. This equation is used to check whether intraparticle diffusion is the sole rate-limiting step [106]. A straight line on a plot of $ln(1 - (\frac{\bar{q}}{q_e})^2)$vs. t passing through the origin indicates IPD is the sole rate-controlling step. More importantly, Eq. (31) is used to determine the IPD coefficient [105,108].

3.3.3. Weber–Morris IPD model

Weber and Morris [111] proposed a model for modeling adsorption kinetics limited by IPD.

$$q = k_{id}\sqrt{t} + B \tag{32}$$

where k_{id} is the IPD rate constant [mg/(g•min$^{0.5}$)], and B is the initial adsorption (mg/g). This model is often referred to as the IPD model.

A plot of q vs $\sqrt{t}$ should be linear. The k_{id} and B correspond to the slope and intercept, respectively. k_{id} generally increases with increasing initial adsorptive concentration [112-114].

This model is the third most common candidate model for liquid adsorption kinetics in environmental remediation after the PFO and PSO models. For kinetics controlled solely by IPD, the line should pass through the origin ($B=0$) [115-117]. However, in most studies, this plot (i) shows multilinearity over the entire adsorption period and (ii) provides better fit if not forced through the origin ($B>0$) [36,118–120].

Multilinearity is an indication of multiple mechanisms that control the process [121]. Each linear segment represents a controlling mechanism or several simultaneous controlling mechanisms. In the initial step, external surface adsorption or instantaneous adsorption occurs. In the second step, IPD begins. In the third step, the system approaches equilibrium. Adsorption slows as surface coverage nears saturation. Given the kinetic data, defining the time period for each line segment is somewhat arbitrary. Piecewise linear regression is helpful in this case [122].

The pore diffusion rate constant decreases from the first step to the last step, thereby signaling the diminishing role of IPD and the increasing role of other mechanisms [123,124]. McKay et al. [125] stated that extrapolation of the linear segment to the ordinate intercept gives a B value that is proportional to the boundary layer thickness. A large B value corresponds to large film diffusion resistance. Raji and Pakizeh [126] found that higher bulk liquid concentration increases both the IPD rate constant and the boundary layer effect indicated by a higher B value.

Douven et al. [127] derived a theoretical background for the Weber–Morris IPD model based on Langmuir surface kinetics. They reported that film diffusion dominates for very short times over the entire adsorption course and can be excluded for model derivation. The range of validity is somewhat more limited than that commonly acknowledged in literature. They found that the IPD model is valid if these conditions are fulfilled: intraparticle control, Henry regime adsorption, and infinite volume of bulk solution.

The initial adsorption behavior at $t=0$ is rarely investigated. Wu et al. reported a decrease in initial adsorption (B value) when smaller adsorbent particles are used [121]. A negative B value in Eq. (32) can be explained by the combined effects of film diffusion and surface reaction control [128].

Used almost exclusively for batch process in the past, the Weber–Morris model was recently applied to a fixed bed setting [129].

3.3.4. Bangham model

Bangham's model assumes IPD to be the only rate-controlling step. It is typically used in the following form [130,131]:

$$\log\left(\log\frac{C_0}{C_0 - q.m}\right) = \log\left(\frac{k_0 m}{2.303V}\right) + \alpha \log t \tag{33}$$

where k_0 and α are constants.

This model has been used to check whether pore diffusion is the sole rate-controlling mechanism. A linear plot of $\log(\log\frac{C_0}{C_0 - q.m})$ vs. $\log t$ is observed if the assumption is true. Pesticide removal by activated carbon was shown to be controlled by pore diffusion in this model [131].

3.3.5. Linear film diffusion model

When the accumulation of adsorptive on the sorbent surface is equal to the adsorptive diffusion rate across the liquid film (boundary layer), as in a film diffusion-dominated system, the bulk liquid phase concentration of adsorptive can be expressed as [132]

$$\frac{dC}{dt} = -k_f(C - C_s) \tag{34}$$

where k_f = film diffusion coefficient (min^{-1}), and C_s = adsorbate concentration at the liquid–solid interface (mg/l). At short times, C_s is negligibly small ($C_s \approx 0$). Eq. (34) can then be integrated to yield

$$\frac{C}{C_0} = \exp(-k_f t) \tag{35}$$

The film diffusion coefficient can be estimated from a plot of $-\ln(C/C_0)$ vs t.

3.3.6. Mixed surface reaction and diffusion-controlled kinetic model (MSRDCK)

Despite good overall linearity in the t/q vs t plot of PSO kinetics, deviation from linearity is spotted in some cases at the initial times of adsorption. A kinetic model that includes the surface reaction and film diffusion control has been developed to correct for this initial time deviation [133].

$$\frac{dq}{dt} = k\left(1 + \frac{\tau^{1/2}}{t^{1/2}}\right)(C_0 - \gamma q)(q_e - q) \tag{36}$$

where $\gamma = \dfrac{(C_0 - C)}{q_e} \tag{36a}$

$$k = \frac{4\pi r_0 D}{\gamma} \tag{36b}$$

$$\tau = \frac{r_0^2}{\pi D} \tag{36c}$$

with r_0 = particle radius (cm); D = film diffusivity (cm^2/min); The integrated form of Eq. (36) is

$$q = q_e \frac{exp(at + bt^{1/2}) - 1}{u_{eq} exp(at + bt^{1/2}) - 1} \tag{37}$$

where $u_{eq} = 1 - C_e/C_0$; C_e = equilibrium concentration of bulk solution (mg/l);

$$a = kC_0(u_{eq} - 1) \tag{37a}$$

$$b = 2kC_0\tau^{1/2}(u_{eq} - 1) \tag{37b}$$

The constants a and b account for surface reaction and diffusion, respectively. This model is able to capture both the initial curved portion of the linear PSO plot and the entire time range of adsorption for dye removal by chitosan and P-g-pAPTAC microspheres [133]. Picloram herbicide adsorption onto montmorillonite clay is best fitted by this mixed model [134].

3.3.7. Multi-exponential model

The multi-exponential model is an attractive candidate model for adsorption kinetics that has multiple parallel routes that contribute to the total adsorbate uptake [135]. In a system with widely different particle sizes, the adsorption kinetics on small and large particles may be controlled by different mechanisms with kinetic parameters that have different orders of magnitude. A similar situation arises when the total uptake is contributed by the adsorption on the sites of widely different energies or on pores of widely different sizes. The multi-exponential model reads

$$q = q_e \left[1 - \frac{\sum_{i=1}^{N} a_i exp(-k_i t)}{\sum_i^N a_i} \right] \qquad (38)$$

where k_i is the rate coefficient for route i (total N route contributing to the total uptake q), and a_i is the weight coefficient that reflects the share of route i.

Chiron et al. used multi-exponential model ($N = 2$, so-called double exponential model) to describe the co-adsorption of Cu(II) and Pb(II) onto amine-grafted silica [136]. Each metal was adsorbed via a two-step mechanism, namely, external particle diffusion and IPD. The k values for lead were nearly double that of copper.

Marczewski et al. [137] used carbon particles of different sizes for organic pollutant adsorption and found a good fit to the kinetic data through a triple-exponential model. Quadruple-exponential fitting was performed by Derylo–Marczewska et al. [138] for dye adsorption on mesoporous carbon.

For $N = 1$, this model is reduced to the PFO model.

3.3.8. Other models

The list of models covered here is by no means comprehensive. Other models that are useful for adsorption or adsorption–diffusion modeling but are not discussed here are parabolic diffusion [139,140], hyperbolic model [141,142], two-site nonequilibrium model [143], branched pore diffusion model [144], nonlinear film transfer model [132], second-order reversible reaction model [145], and mixed-order rate equation [146,147], among others.

4. Correlating the kinetic data

4.1. Linear fitting vs. nonlinear fitting

Linear regression analysis is simple to implement and is applicable to a broad array of kinetic adsorption systems [16]. The usual practice in environmental adsorption studies is to fit the linearized form of PFO, PSO, and other relevant models to the data sets. The best-fit model is determined based on the correlation of determination (R^2) value, and the obtained model parameters are cross-checked with the experimental values. One problem is that different linearized forms of the PSO model provide sometimes-widely different parameter values [117]. Nonlinear regression is recommended to circumvent this problem, and it has been shown to be better than linear regression such that more realistic values of q_e and k values, and often a higher correlation coefficient (R^2) value are obtained [24]. A similar situation applies to PFO kinetics modeling and breakthrough modeling [148].

During nonlinear regression, model parameters are first estimated and then continuously evolve toward the values that minimize a predefined error function. This evolution is based on a selected optimization algorithm (e.g., Levenberg–Marquardt algorithm), which determines how the estimated set of values converges toward their final optimized values [149]. Despite the accuracy and consistency of nonlinear regression over linear regression, its popularity does not penetrate deep into the community.

A large number of works disregard PFO in favor of PSO as an outcome of model discrimination by linear regression based on the marginal differences in R^2 values. Some publications caution against this unscrupulous discrimination [11]. First-order kinetics, which has been ascribed to PSO by linear regression, surprisingly fits PFO by nonlinear regression [150].

Fit quality depends on the experimental error and range of time. Linearized PFO shows better fit for initial periods than later times [11]. In addition, PFO is prone to experimental error, whereas PSO is less sensitive to experimental error. A large experimental error can make the right model fit poorly and the wrong model fit

adequately, thereby providing misleading kinetic information. Fortunately, the nonlinear forms of kinetic models are more robust toward experimental errors and are hence preferred, especially when experimental errors are not controlled.

The effect of linearizing a model is altered error distribution of the data set. Linear regression yields a Gaussian distribution of the errors in the data set. However, the linearized data set might have a distorted error distribution if plotted on linearized axial settings by using the model parameters determined from the nonlinear method [151,152]. One concrete evidence of this error structure distortion is in the PSO linear plot. The ordinate t/q value is undefined at $t = 0$ because q is supposedly zero. Applying linear regression will force the error distribution to be Gaussian by defining new values for the model parameters, which can be different and even illogical [55,153]. Different linear transformations modify the error structure differently. Hence, careful choice of the linearized form is advised.

At least five linearized forms of PSO are available [49]. Kumar [150] found that the most popular form of PSO (t/q vs. t) was not the best form. Ho [49] and Nouri et al. [154] found that the most commonly used form is the best linearized form that yields the most accurate and reliable parameter values, second only to those obtained by the nonlinear regression method. This difference shows that the accuracy of the linearized form and the linearization-induced numerical error are dependent on the adsorbent–adsorbate type and experimental conditions.

To the best of our knowledge, no thorough analysis of the linearization issues has been reported for kinetic adsorption models. This condition can be attributed to two factors. First, the primary interest of most studies lies in materials development and evaluation, and not on model development. Second, benchmark values against which the obtained parameters from linear and nonlinear analyses can be confidently compared are insufficient. The best at hand for the community is experimental equilibrium capacity. However, adsorption systems that take a long time to saturate add further complexity to the determination of equilibrium capacity and its subsequent verification by models [155,156].

Whether linear or nonlinear regression is used for model fitting is not clearly reported in some works. This obscurity is regrettable because the linear or nonlinear method can affect the accuracy of the fitted parameters and, more importantly, the eventual model attribution of the data set. Such works prevent any meaningful comparisons by upcoming similar works.

Malpractices are common to the point of gaining ground in liquid systems modeling [43]. In addition to the aforementioned linearization issue, these malpractices include inappropriate data fitting (selective or forced fitting) and statistical discrimination bias.

With the advent of computing technology, nonlinear regression has become less of a hassle and should therefore be prioritized over the linear method. Whenever possible, a comparison should be made between the linearized and nonlinear models in terms of fit quality and reasonability of the determined parameters before deciding on the best model.

4.2. Error functions

Error functions are statistics that quantify the error between the model parameters and experimental values. Linear regression is a standard method developed based on the least squares criterion [157]. Model parameters are captured well by the slope and intercept, both of which are clearly defined as functions of the experimental data. The fitted parameters are set by regression to minimize the sum-of-squares errors between the predicted and experimental values. In standard nonlinear regression, the fitted parameters are also set to minimize the sum-of-squares errors [149]. However, other error functions can be defined as the objec-

tive function in place of the most commonly used least squares function for data regression. Unlike linear regression, nonlinear regression is an iterative procedure, during which model parameters values are iterated based on a chosen algorithm to minimize the predefined error function (R^2 is to be maximized) [49]. This regressive iteration is conveniently accomplished by using computing software, such as Matlab, OriginPro, Mathematica, and SPSS.

In the literature, these error statistics are calculated in addition to the correlation of determination (R^2) to confirm and support the model already discriminated by R^2. High R^2 values correspond to low error statistics in most cases. When the R^2 values are too close to discriminate the PFO and PSO models, RMSE (see Eq. (42) for definition) comes in handy [158]. El-Khaiary and Malash [43] raised a concern about the possible bias in taking R^2 as the goodness-of-fit criterion for models that have different degrees of freedom.

Some notable error functions are listed as follows. The coefficient of determination is restricted to $0 < R^2 \leq 1$. An R^2 value closer to unity indicates a better fit. A detailed discussion about these statistics is presented elsewhere [159,160].

For Eqs. (39)–(48) and (48a), the notation is: q_{cal}=model-predicted value and q_{exp}=experimental value. Subscript i is omitted from q_{cal} and q_{exp} for clarity.

(1) Sum-of-squares of errors (SSE)

$$SSE = \sum_{i=1}^{n} (q_{cal} - q_{exp})^2 \tag{39}$$

(2) Chi-squared statistic, χ^2

$$\chi^2 = \sum_{i=1}^{n} \frac{(q_{exp} - q_{cal})^2}{q_{cal}} \tag{40}$$

(3) Mean sum-of-squares error (MSE)

$$MSE = \frac{1}{n} \sum_{i=1}^{n} (q_{cal} - q_{exp})^2 \tag{41}$$

(4) Root mean sum-of-squares error (RMSE)

$$RMSE = \sqrt{\frac{1}{n} \sum_{i=1}^{n} (q_{exp} - q_{cal})^2} \tag{42}$$

(5) Normalized standard deviation, Δq (%)

$$\Delta q(\%) = 100 \sqrt{\frac{1}{n-1} \sum_{i=1}^{n} \left(\frac{q_{exp} - q_{cal}}{q_{exp}} \right)^2} \tag{43}$$

This function is also known as average relative standard error (ARS).

(6) Average relative error (ARE)

$$ARE = \frac{1}{n} \sum_{i=1}^{n} \left| \frac{q_{exp} - q_{cal}}{q_{exp}} \right| \tag{44}$$

(7) Coefficient of determination (a.k.a. correlation coefficient) (R^2)

$$R^2 = \frac{\sum_{i=1}^{n} (q_{cal} - \overline{q_{exp}})^2}{\sum_{i=1}^{n} (q_{cal} - \overline{q_{exp}})^2 + \sum_{i=1}^{n} (q_{cal} - q_{exp})^2} \tag{45}$$

An adjusted R^2 is used to eliminate the goodness of fit contributed by (large) sample size and gauge the intrinsic fit quality.

$$\text{Adjusted } R^2, = 1 - (1 - R^2) \cdot (n-1)/(n-1-p) \tag{46}$$

P = number of model parameters

(8) Sum of absolute error (SAE)

$$SAE = \sum_{i=1}^{n} |q_{cal} - q_{exp}| \tag{47}$$

(9) Marquadt's percent standard deviation (MPSD)

$$MPSD = 100 \sqrt{\frac{1}{n-p} \sum_{i=1}^{n} \left(\frac{q_{exp} - q_{cal}}{q_{exp}} \right)^2} \tag{48}$$

A modified MPSD is

$$F_{error} = \sqrt{\left(\frac{1}{n-p} \right) \sum_{i=1}^{n} (q_{exp} - q_{cal})^2} \tag{48a}$$

5. Modeling works on batch adsorption systems

In this section, representative works are selected from the literature for an overview of the current state. General trends are discussed, and interesting findings are mentioned. The kinetic investigations of adsorption systems that involve the removal of heavy metal ions from water are provided in Table 1. The modeling studies of selected adsorption systems that involve the aqueous-phase removal of other pollutant categories are tabulated in Tables 2–5, and 6. The best-fit model is emboldened. For such diverse adsorption systems, PSO exhibits good fit over the entire time course, thereby showing its ability to depict, by its own, various mechanisms.

5.1. Heavy metals

Table 1 lists the adsorption systems where heavy metal ions are removed from water. The adsorbents are representative of the major classes in the literature. The adsorbent dose ranges from 0.01 g/l to 200 g/l, while the initial concentration ranges from 50 ppm to 500 mg/l. Despite this wide range, PSO prevails over PFO in most cases. For lead-sawdust [37] and chromium-hydrotalcite [161] adsorption systems, both pseudo models provide comparable fit goodness (i.e., R^2 value). PFO is selected because the predicted q_e agrees better with the experiment. The works in Table 1 shows that no distinct set of conditions that favor the PFO can be observed. The Weber–Morris plot rarely passes through the origin. For metal adsorption onto $CaCO_3$–maltose hybrid adsorbent, the first segment of the multilinear line passes through the origin [116].

5.2. Dyes

Table 2 shows the adsorption systems in which synthetic dyes are removed from water. Similar to heavy metals, PFO-compliant kinetics is difficult to come by. The attribution of the adsorption systems to PSO could be decided by a matching q_e value when the R^2 values are quite close [102,183-185]. Hameed and El-Khaiary [102] found from Boyd's plot that the diffusion coefficient, D, decreases with the increase in dye concentration. The general order model best describes the uptake of reactive violet 5 by cocoa shell activated carbon, dictated by the highest R^2_{adj} and lowest modified MPSD [96]. The order of reaction increases with initial adsorptive concentration and ranges between 1.20 and 1.38. How much this mathematical advantage boosts its profiling of the uptake kinetics is unclear because the general order model is a three-parameter model (as opposed to the two parameters of PFO or PSO).

5.3. Phenolics

Table 3 shows some works on the removal of phenol and phenolic compounds from wastewater. The PFO correlates the kinetics

ARTICLE IN PRESS

Table 1
Selected works on the removal of heavy metal ions from water.

Adsorbate	Adsorbent	Adsorbent dose (g/l)	Temperature (°C)	Initial adsorptive concentration, C_0(mg/l, except otherwise stated)	Experimental uptake, q_{exp}(mg/g, except otherwise stated)	Candidate model (the best fit model(s) in bold)	Discrimination	Reference
Cr	Calcined Mg–Al–CO$_3$ hydrotalcite	0.5	30	10	20	**PFO**, PSO	R^2, χ^2	[161]
Pb	Biomass-added crosslinked chitosan beads	200	20	73.4	0.28	**PFO**, PSO	R^2	[162]
Ni	Polyurethane foam	10	30	50	2.18	PFO, **PSO**	R^2	[163]
Pb	Carbonized rubber waste sawdust	0.5	30	20	35.8	**PFO,** PSO, IPD	R^2	[37]
Pb	Zeolite–NaX	12	30	10	90% removal	**PFO**, PSO, **first order reversible reaction model**, Elovich, Bangham, IPD	R^2	[164]
Cu; Mn; Pb	Pecan nutshell	5; 5; 4	25	300; 300; 300	85; 95.2; 175.5	**Avrami fractionary order**, PFO, PSO, Elovich, IPD	R^2; Δq	[92]
Pb	Acid activated bentonite	10	30	5	0.330	PFO, **PSO**, IPD	R^2,RMSE	[165]
Pb; Hg	Functionalized magnetic mesoporous silica	0.01; 0.01	25	1; 1	0.43 mmol/g; 0.5 mmol/g	**PSO**, IPD	–	[166]
Cd, Cu, Pb. Zn	Chestnut shell	10; 10; 10; 10	25	100; 100; 100; 100	9.86; 9.61; 8.81; 9.26	**PSO**, IPD	R^2, Δq	[117]
Pb; Ni; Mn Cu; Co; Cd;	CaCO$_3$–maltose hybrid	4/7; 4/7; 4/7; 4/7; 4/7; 4/7;	–	811.5; 43.8; 565.2; 572.4; 43.4; 410.1	1884.2; 37.4; 332.5; 566.9; 63.5; 367.5	PFO, **PSO**, IPD	R^2	[116]
Pb	Low silica nano-zeolite X	1.5	45	15	789.12	PFO, **PSO**	R^2	[167]
Re(VII); Mo(VI)	Modified waste paper gel	2; 2	30	20; 20	0.96 mmol/g; 4.99 mmol/g	PFO, **PSO**	R^2	[168]
As	Pine leaves	20	25	10	0.0232	PFO, **PSO**	R^2	[169]
Cu	Diamine-modified mesoporous silica on multiwalled carbon nanotube (MWCNT)	1	25	100	45	**PSO**, IPD	R^2	[124]
Cd; Pb	Sodic bentonite clay	10; 10	20	0.394 mmol/l; 0.394 mmol/l	0.038 mmol/g; 0.035 mmol/g	PFO, **PSO**, IPD	R^2, χ^2, RMSE	[170]
Pb	Weak acidic cation resin	1	25	50	47.75	PFO, **PSO**, IPD, external diffusion model, pore- surface mass diffusion model	R^2,ARE	[108]
Hg	Mercapto-grafted rice straw	1	50	0–400	45.3	PFO, **PSO**, Elovich, IPD, Pore diffusion model, Film diffusion model	R^2, Δq	[60]

Table 1 (continued)

Adsorbate	Adsorbent	Adsorbent dose (g/l)	Temperature (°C)	Initial adsorptive concentration, C_0(mg/l, except otherwise stated)	Experimental uptake, q_{exp}(mg/g, except otherwise stated)	Candidate model (the best fit model(s) in **bold**)	Discrimination	Reference
Hg	Sugarcane bagasse	5	30	76	14.7	PFO, **PSO**	R^2	[171]
Hg	Palm shell activated carbon	2	30	200	69.35	PFO, **PSO**, IPD	R^2	[172]
Cd	Ionic imprinted silica-supported hybrid adsorbent	4	25	300	29.1	PFO, **PSO**, Elovich, IPD	R^2	[173]
Pb;	Tea waste	0.6;	25	20;	26.33;	**PSO**	R^2	[174]
Cd;		0.6;		20;	11.58;			
Cu		0.6		20	15.62			
Thallium(I)	Prussian blue immobilized on alginate capsules	0.4	–	50	54.7	PFO, **PSO**, Crank model	MSE	[175]
Hg	MCM-41 modified by ZnCl$_2$	1/3	20	50	87	PFO, **PSO**, Elovich, IPD, Dumwald Wagner, Crank	R^2	[126]
Pb	Iron-loaded ash nanoparticles	0.1	25	25–200	822.5	PFO, **PSO**, IPD, Elovich	R^2	[176]
Pb	Polyacrylamide Zr(IV) iodate	10	50	200	5.57	PFO, **PSO**, IPD	RMSE,SAE, χ^2,Δq	[120]
Pb	Activated carbon/Fe$_3$O$_4$@SiO$_2$–NH$_2$	0.8	30	100	81.3	PFO, **PSO**	R^2	[177]
Cd;	Polyaniline grafted	4.5;	25	220;	98.45;	PFO, **PSO**	R^2, χ^2	[178]
Pb	crosslinked chitosan	4.5		220	90.45			
Cd	Corn stalk xanthates	5	40	100	9.86	PFO, **PSO**	R^2	[179]
Pb	Metal organic framework MIL-101 functionalized by ethylenediamine	1	25	500	70.42	PFO, **PSO**, IPD	R^2	[180]
Pb	Ethylenediaminetetraacetic acid -Zr(IV)iodate	10	25–50	10–60	26.04	PFO, **PSO**, IPD, Elovich	R^2	[33]
Hg	Montmorillonite modified with dimercaprol;	2;	30	10	3.179;	PFO, **PSO**	R^2	[181]
	Vermiculite clay modified with dimercaprol	2			4.9605			
Cu;	Layered double hydroxide intercalated with MoS$_4^{2-}$ ion	1.2;	25	20–30ppm	17;	PFO, **PSO**	R^2	[182]
Ag;		1.2;			16;			
Pb;		1.2;			16;			
Hg		1.2			24			

ARTICLE IN PRESS

Table 2
Selected works on dyes removal from water.

Adsorbate	Adsorbent	Adsorbent dose (g/l)	Temperature (°C)	Initial adsorptive concentration, C_0 (mg/l, except otherwise stated)	Experimental uptake, q_{exp} (mg/g)	Candidate model (the best fit model(s) in bold)	Discrimination	Reference
Methylene blue	Broad bean peels	1.5	30	325	167.52	**PFO**, PSO	R^2	[185]
Malachite green	Oil palm trunk fiber	1.5	30	300	97.78	**PFO**, PSO, IPD, Elovich, Boyd	R^2	[102]
Malachite green	Maize husk leaf	2.5	50	200	73.9	**PFO**, PSO	R^2	[183]
Methylene blue	Zeolite NaA	1	30	120	50.7	**PFO**, PSO, IPD	R^2	[184]
Methylene blue; Methyl orange	Mesoporous carbon	–	–	–	0.107; 0.115	PFO, PSO, **multi-exponential model**	R^2, modified RMSE	[138]
Methyl red	Metal organic framework MIL-53(Fe)	0.1	25	100	76.94	PFO, **PSO**, IPD	R^2	[186]
Congo red	Polypyrrole-polyaniline nanofiber	1	25	100	100	PFO, **PSO**, IPD	R^2	[187]
Basic yellow 28	Calcined eggshell	2	25	50	23.31	PFO, **PSO**	R^2	[188]
Reactive violet 5	Cocoa shell activated carbon	2.5	25	1000	399	PFO, PSO, **general order model**, IPD	R^2, R^2_{adj}, modified MPSD	[96]
Malachite green	Graft copolymer derived from amylopectin and poly(acrylic acid)	2	35	500	245.098	PFO, **PSO**, Second order, IPD	R^2, χ^2	[113]
Acridine orange; Rhodamine 6G	Food waste hydrochar	0.5; 0.5	40	50; 50	99.323; 94.277	PFO, **PSO**	R^2, χ^2	[189]
Methylene blue	Poly(cyclotriphosphazene-co-4,4′-sulfonyldiphenol) nanotube	0.75	25	100	69.16	PFO, **PSO**, IPD	R^2	[118]
Basic blue 41	Nanoporous silica	0.5	30	60	113.264	PFO, **PSO**, IPD	R^2	[35]
Methylene blue	Methyl-functionalized mesoporous silica	1	45	2.5–20	15.87	PFO, **PSO**, IPD	R^2	[190]
Orange II	Surfactant coated zeolite	4	35	250	59.17	**PSO**	R^2	[191]
Basic Fuchsin dye	Calcined mussel shell	5	25–155	200	186.67	PFO, **PSO**, IPD	R^2, χ^2, MSE, Δq	[192]
Methylene blue	Magnetic metal organic framework Fe_3O_4–$Cu_3(BTC)_2$	1	30–50	100	84	PFO, **PSO**	R^2	[193]
Methylene blue; Methyl orange	Montmorillonite-pillared graphene oxide	0.5; 4	30	150; 50	345.0; 131.8	PFO, **PSO**, IPD	R^2, S^2 (unexplained)	[194]
Acid brilliant scarlet	Crab shell waste activated carbon	0.5	20	500	988.5	PFO, **PSO**, Elovich, IPD	R^2	[195]
Malachite green	Tetraethylenepentaamine functionalized activated carbon	0.2	25	50	217.175	PFO, **PSO**, IPD	R^2	[196]
Procion blue PB;Remazol brilliant blue R	Bentonite-Mg(OH)$_2$ composite	2; 2	25	120; 120	40.4; 47.21	PFO, **PSO**	R^2	[32]
Eriochrome black T	Crosslinked polyzwitterionic acid	1.5	25	10ppm	4.07	PFO, **PSO**	R^2	[197]
Rhodamine B	Activated carbon from biomass gasification residue	0.05	25	20	215.7	PFO, **PSO**, IPD, Elovich	R^2	[198]

Table 3
Selected works on the removal of phenolics from water.

Adsorbate	Adsorbent	Adsorbent dose (g/l)	Temperature (°C)	Initial adsorptive concentration C_0 (mg/l, except otherwise stated)	Experimental uptake, q_{exp} (mg/g, except otherwise stated)	Candidate model (the best fit model(s) in bold)	Discrimination	Reference
Phenol	Commercial activated carbon	2	25	100	45	**PFO**, PSO, IPD	R^2	[199]
4-chlorophenol	Surfactant modified montmorillonite clay	3	25	100	29.96	PFO, **PSO**, IPD	R^2	[200]
Phenol; 4-chlorophenol; 2,4-dichlorophenol	Pistachio shell activated carbon	1; 1; 1	30	1000 mmol/l	3.04 mmol/g; 3.35 mmol/g; 3.83 mmol/g	PFO, **PSO**	R^2, Δq	[201]
4-nitrophenol	Mansonia sawdust	1.5	26	0.8628 mmol/l	0.1242 mmol/g	PFO, **PSO**,IPD, Boyd, Double exponential	R^2	[202]
Phenol	Natural zeolite	2	25	90	32.6	PFO, **PSO**, IPD	R^2	[36]
Phenol	N-methylacetamide modified hypercrosslinked resin	4	25	1020	180	PFO, **PSO**	R^2	[203]
Phenol	Chitin	4	25	41.4	7	PFO, **PSO**, IPD	R^2	[204]
Phenol	Zeolite X/activated carbon composite	6	25	552.12	30.52	PFO, **PSO**, IPD	R^2	[205]
Bisphenol A	Montmorillonite clay modified by surfactant	7.5	25	100	0.078 mmol/g	PFO, **PSO**	R^2	[206]
Pentachlorophenol	Fe$_3$O$_4$@SiO$_2$ MWCNT	0.5	25	50	35.58	PFO, **PSO**	R^2	[25]
Phenol	Activated carbon (AC)	1	30	1000	212.47	PFO, **PSO**, IPD	R^2, Δq	[123]
2,4 Dichlorophenol	Montmorillonite clay	10	30	100	9.8	PFO, **PSO**	R^2	[207]
Phenol	MWCNT	5	25	25	4.36	PFO, **PSO**, IPD	R^2	[208]
Bisphenol AF	Chitosan modified zeolite	1	25	0.1 mmol/l	0.078 mmol/g	PFO, **PSO**, Elovich, IPD	R^2	[209]
Phenol	Polymeric resin Amberlyst A26	7	25	200	20	PFO, **PSO**	R^2, SSE	[114]

of phenol adsorption in a multistage external loop airlift reactor [199]. In this reactor setup, air bubbles are sparged through the solution at a superficial velocity of 2.19 cm/s to enhance mass transfer. As in all other surveyed phenolics works, PSO fits better than the other models.

5.4. Pesticides

Table 4 shows some selected works on the adsorptive removal of pesticides from water. Out of the 16 surveyed papers, two papers reported that PFO is better than PSO [131,210], and one paper reported that both are equally acceptable [24]. Boyd's equation was used to determine the effective diffusion coefficient, which decreases with the increase in initial pesticide concentration [210]. PFO produces convincing q_e and R^2 values for the adsorption onto waste rubber tire activated carbon [131]. Marco–Brown et al. [134] applied the mixed surface reaction and diffusion-controlled kinetic model to picloram herbicide adsorption on montmorillonite. The downward curvature at the initial times of the linear PSO plot warrants the application of the mixed surface reaction and diffusion-controlled kinetic model. According to this model, the lack of fit at the initial period is a diffusion effect. All other cases in Table 4 are fitted well by PSO.

5.5. Pharmaceuticals, personal care products, and endocrine disruptors

This class of pollutants is gaining attention in environmental adsorption due to their growing presence in water bodies. Table 5 provides some modeling works on this rising class of pollutants. Some noteworthy findings are summarized below.

(i) PFO does not converge for three pharmaceuticals, namely, carbamazepine (CBZ), oxazepam (OXZ), and piroxicam (PIR), on non-activated carbon prepared from paper mill sludge [221]. However, it converges for the adsorption of those pharmaceuticals on commercially activated carbon and performs better than PSO for the adsorption of OXZ and PIR.

(ii) Dimetridazole (DMZ), which has the smallest molecules in the study, fits PFO better [222]. By contrast, trinidazole (TNZ), which has the largest molecules in the study, fits PSO better.

(iii) In the presence of sodium dodecylsulfate surfactant, the rate constant k_2 increases with the initial concentration of Thioridazine hydrochloride (THCl) [223], whereas k_2 decreases at higher initial THCl concentration in the absence of surfactant.

5.6. Other pollutants

Table 6 shows other common pollutant adsorption kinetics. For the kinetics of phosphate removal, PFO and PSO fit equally well [115]. The first portion of the IPD curve passes through the origin, thereby indicating IPD control at the initial period of adsorption [115]. In the case of Patulin adsorption, PFO with an R^2 value of 0.8885 outperforms PSO [234].

6. Modeling the kinetics of fixed bed adsorption

6.1. Breakthrough curve

Industrial adsorption processes typically run in continuous mode in fixed bed [239,240]. Breakthrough curve is the plot of concentration versus time at the column exit. Polluted stream passes through the column packed with fixed bed of adsorbent particles. As the pollutants are adsorbed in the bed, cleaned stream

ARTICLE IN PRESS

Table 4
Selected works on pesticides removal from water.

Adsorbate	Adsorbent	Adsorbent dose (g/l)	Temperature (°C)	Initial adsorptive concentration C_0 (mg/l, except otherwise stated)	Experimental uptake, q_{exp}(mg/g, except otherwise stated)	Candidate model (the best fit model(s) in bold)	Discrimination	Reference
Monocrotophos	Waste jute fiber carbon	0.5	28	40	39.84	**PFO**, PSO, IPD, Boyd	R^2,SSE	[210]
Methoxychlor; Atrazine; Methyl parathion	Waste rubber tire AC	0.1; 0.1; 0.1	25	12; 12; 12	112; 104.9; 88.9	**PFO**, PSO	R^2	[131]
Carbofuran	Rice husk biochar	1	30	50	24.6	**PFO, PSO**, Elovich, IPD	R^2, χ^2	[24]
2,4-dichlorophenoxyacetic acid	Pumpkin seed hull AC	1	30	400	253.56	PFO, **PSO**	R^2_{adj}; RMSE	[211]
Diuron	Volcanic ash derived soil	200	30	5 µg/l	43.4 µg/g	Hyperbolic model, PFO, **PSO,** Elovich, Boyd, IPD, two-site nonequilibrium model	R^2	[212]
Bentazon	Fruit husk AC	1	30	250	131.08	PFO, **PSO**, IPD	R^2	[67]
Mesosulfuron-methyl	Propyl sulfonic acid functionalized phenyl-periodic mesoporous benzene-silica	2	25	20	9.68	**PSO**	R^2	[213]
Picloram	Montmorillonite clay	16	25	5 mmol/l	Fractional uptake is measured instead of absolute uptake	PFO, PSO, **MSRDCK**, IPD	R^2	[134]
2,4-dichlorophenoxyacetic acid	Combustion-synthesized carbon	2	25	0.5 mmol/l	0.245 mmol/g	PFO, **PSO**, IPD	R^2	[214]
Paraquat; Amitrole	Organomontmorillonite modified by zwitterionic surfactant	3.2; 3.2	45; 5	300; 40	74.0058; 3.6502	PFO, **PSO**	R^2,SSE	[215]
Glyphosate; Glufosinate	Metal organic framework UiO-67	0.03; 0.03	25	0.1 mmol/l; 0.1 mmol/l	1.9 mmol/g; 0.87 mmol/g	PFO, **PSO**, IPD	R^2	[216]
2,4-dichlorophenoxyacetic acid	Iron oxide nanoparticles doped carboxylic ordered mesoporous carbon	1	30	500	312.54	PFO, **PSO**	R^2_{adj}; RMSE	[217]
Fenarimol	Magnetic iron oxide/Polygorskite clay composite nanoparticles	10	20	5	344 µg/g	PFO, **PSO**, IPD	R^2,standard errors of estimates	[218]
Mesosulfuron-methyl	HMOR zeolite	2	25	8	3.4	**PSO**	R^2	[219]
Thiamethoxam; Acetamiprid; Imidacloprid; Primicarb	Acid-treated chestnut shell	20	25	10	0.2777; 0.3227; 0.3462; 0.4196	PFO, **PSO,** IPD	R^2, modified RMSE	[220]
Dicamba	Loponite-starch derived mesoporous carbon	0.5	25	250	220	PFO, **PSO**, IPD	R^2	[119]

Table 5

Selected works on the removal of PPCPs from water.

Adsorbate	Adsorbent	Adsorbent dose (g/l)	Temperature (°C)	Initial adsorptive concentration C_0 (mg/l, except otherwise stated)	Experimental uptake, q_{exp} (mg/g, except otherwise stated)	Candidate model (the best fit model(s) in bold)	Discrimination	Reference
Thioridazine hydrochloride (THCl)	Activated charcoal	0.1	25	0.4 mmol/l	0.750 mmol/g	PFO, **PSO**, IPD	R^2	[223]
Dimetridazole; Metronidazole; Ronidazole; Trinidazole	Commercial AC and petroleum coke AC	0.2; 0.2; 0.2; 0.2	25	150	2.1; 1.703; 1.762; 1.508	PFO, **PSO**, diffusion model	R^2	[222]
Diphenhydramine	Montmorillonite clay	5	22	1000	0.66 mmol/g	PFO, **PSO**, Elovich, parabolic diffusion	R^2	[224]
Amoxicillin	Quaternized cellulose from flax noil	0.4	50	80	130.89	PFO, **PSO**, Elovich, IPD	R^2	[225]
Ciprofloxacin; Norfloxacin	Biomass AC	0.75; 0.75	30	100; 100	107; 165.02	PFO, **PSO**, IPD	$R^2, \Delta q$	[226]
Ibuprofen; Clofibric acid	Bamboo waste AC	2; 2	25	120; 120	61.6; 55.20	PFO, **PSO**, IPD	$R^2; \Delta q$	[227]
Cephalexin; Cefixime	MgO nanoparticles	0.45	20	200	184.9; 171.6	PFO, **PSO**, IPD	R^2	[228]
Ciprofloxacin	Layered chalcogenides	0.133	25	50	204.31	PFO, **PSO**, IPD	R^2	[229]
Sulfamethazine; Chloramphenicol	N-doped porous carbon	0.3	45	150; 150	487.5; 490	PFO, **PSO**, IPD	R^2	[230]
Tetracycline	Petroleum coke AC	0.1	50	100	995.79	PFO, **PSO**, IPD	R^2	[231]
Diclofenac; Nimesulide	Cocoa shell AC	2.5; 2.5	25	150	51.63; 57.49	PFO, PSO, **general order model**	R^2_{adj}; Standard deviation	[95]
Prami; Dorzo	Oxidized potato peel	1; 1	25	50	31.1; 30.4	PFO, **PSO**	R^2	[232]
Carbamazepine; Oxazepam; Sulfamethoxazole; Piroxicam; Cetirizine; Venlafaxine; Paroxetine	non-activated carbon prepared from paper mill sludge	0.15; 0.25; 0.25; 0.25; 0.4; 2.0	25	5	10.1; 12.4; 1.45; 5.03; 7.9; 9.2; 24.9	PFO, **PSO**	R^2, S_{yx} (unexplained)	[221]
Ibuprofen; Tetracycline	Ricehusk AC; Peach stone	2.4; 2.4	30	100; 100	42.7; 41.7	PFO, **PSO**, Elovich, IPD	R^2	[233]

Table 6
Selected works on the removal of other pollutants from water.

Adsorbate	Adsorbent	Adsorbent dose (g/l)	Temperature (°C)	Initial adsorptive concentration, C_0 (mg/l)	Experimental uptake, q_{exp} (mg/g)	Candidate model (the best fit model(s) in bold)	Discrimination	Reference
Patulin	Thiourea-modified chitosan resin	2	25	7	2.0965	**PFO**, PSO, liquid film diffusion, IPD	R^2	[234]
Phosphate	Chitosan beads modified with zirconium(IV) ions	0.2	15	30	64.14	**PFO**, **PSO**, particle diffusion, IPD, Elovich	R^2	[115]
Etherdiamine	Sugarcane bagasse modified with succinic anhydride; sugarcane bagasse modified with EDTA dianhydride	0.5; 0.5	25	450	509.47; 320.90	PFO, **PSO**, Elovich	R^2	[235]
Naphthalene	Divinylbenzene resin	2	25	30	11.84	PFO, **PSO**	R^2	[236]
Perfluorooctane sulfonate; Perfluorooctanoate	Polyaniline nanotube	0.2;	34	500	980; 650	PFO, **PSO**	R^2	[237]
Linear alkyl benzene	Functionalized MWCNT	1	24	4.0	39.18	PFO, **PSO**, IPD	R^2	[238]
Fluoride	Metal Organic framework UiO-66-NH$_2$	0.5	20	20	22.82	PFO, **PSO**,IPD	R^2	[59]

is produced at the column exit. The concentration of pollutants in the column effluent will increase with time because of the limited adsorption capacity in the bed. Fig. 2 shows a typical breakthrough curve. The gray-colored zone is the mass transfer zone where adsorption takes place and concentration varies axially. Breakthrough occurs (at time t_b in Fig. 2) when the leading front of this zone (called mass transfer front) reaches the column exit. The normalized breakthrough concentration C_b/C_0 is arbitrarily defined at $C_b/C_0 = 0.05$ in Fig. 2. If high-purity raffinate (effluent) is the desired product, then the breakthrough concentration marks the maximum permissible limit of the raffinate concentration.

The breakthrough experiment is important because this is the most probable mode on which any candidate adsorbent will be run should they become commercialized. Therefore, dynamic column breakthrough experiment is important for evaluating newly developed adsorbents. The capacity of the bed can be calculated from the breakthrough curve via mass balance [241]

$$q = \frac{QC_0 \int_{t=0}^{t=\infty} 1 - \frac{C}{C_0} dt - \varepsilon \frac{\pi D^2 L}{4} C_0}{m} \tag{49}$$

where $q=$adsorbed amount per unit mass of adsorbent (mg/g), $Q=$feed flowrate (ml/min), $C_0=$feed concentration (mg/ml), $C=$effluent concentration (mg/ml), $D=$column diameter (cm), $L=$bed height (cm), $\varepsilon=$bed void fraction (cm^3 void/cm^3 bed), $m=$adsorbent mass (g), and $t=$time (min). The second term is a correction term that accounts for the non-adsorbed adsorptive remaining in the voids of the bed. In the liquid adsorption literature, the correction term is often dropped. This condition can be acceptable only if the correction term is much smaller than the first term.

The shape of the breakthrough curve reveals important information on the mass transport dynamics and adsorption kinetics [242]. Factors that influence the kinetics would influence the shape of the breakthrough curve. A more dispersed curve is usually ascribed to higher mass transfer resistance [242], and shorter breakthrough time indicates a lower bed capacity [108,233].

The equilibrium loading for a bed section varies with time. Initially, the mid-column establishes equilibrium with a very dilute solution. As the mass transfer zone progresses to the mid-column (Fig. 2), the solution concentration that passes through the mid-column becomes increasingly concentrated, and the mid-column will then have to establish equilibrium with an increasing solution concentration. This flow-through adsorption is called dynamic adsorption, as opposed to batch adsorption, which is static.

The study of column breakthrough dynamics involves simultaneously solving three conservation equations [243]: (1) mass balance, (2) energy balance, and (3) momentum balance. These balance equations are usually derived from physical situations and cast in partial differential equations form. For liquid phase studies, heat effects and pressure drop are negligible. Therefore, only mass balance needs to be solved. The mass balance equation is

$$\frac{\partial C}{\partial t} + v \frac{\partial C}{\partial z} + \frac{1-\varepsilon}{\varepsilon} \rho_p \frac{\partial q}{\partial t} = D_L \frac{\partial^2 C}{\partial z^2} \tag{50}$$

where $v=$interstitial liquid velocity (cm/s), $\rho_p=$adsorbent particle density (g/cm^3), $D_L=$ axial dispersion coefficient (cm^2/s), and z is the spatial coordinate for the column length (cm). A suitable rate equation for $\frac{\partial q}{\partial t}$ is required. A simple rate equation is the linear driving force (LDF) model

$$\frac{\partial q}{\partial t} = k(q_e - q) \tag{51}$$

In continuous adsorption, q_e is a variable in space and time, constrained by the equilibrium isotherm. Eq. (51) is actually PFO, but the k value here is a transport parameter (mass transfer coefficient). If Langmuir surface kinetics is assumed, then

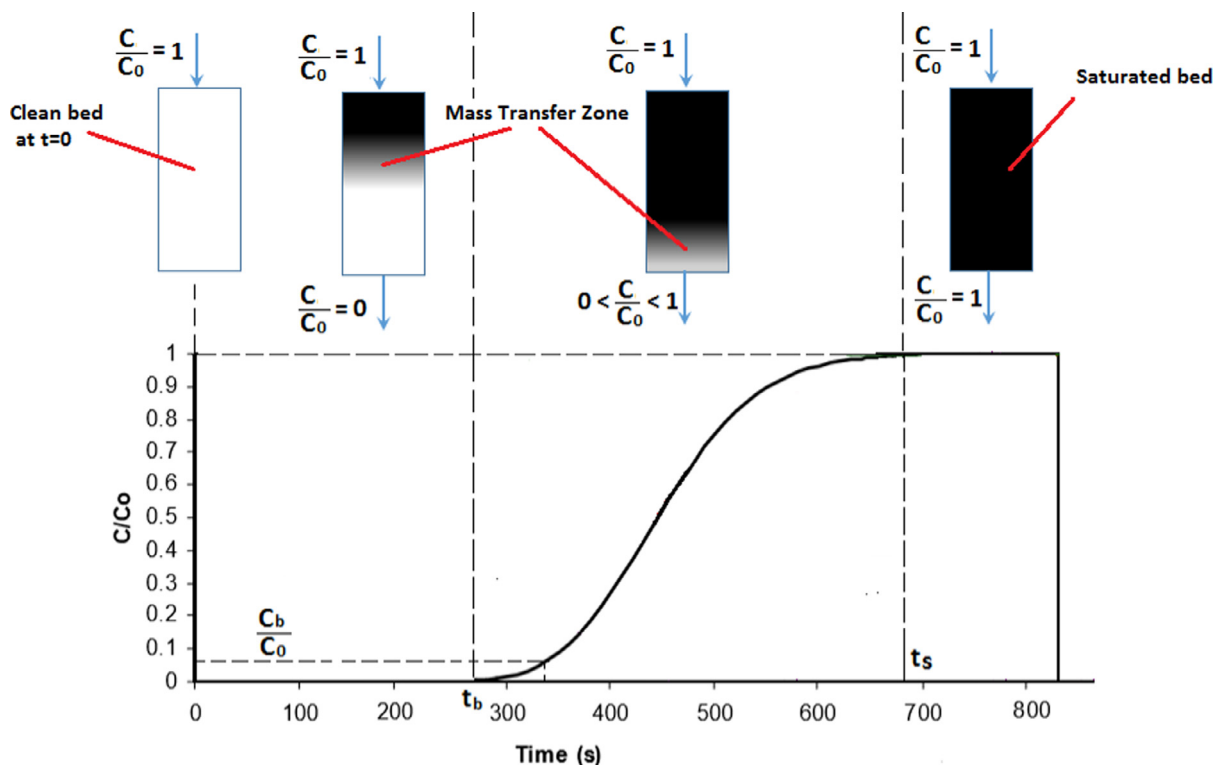$$\frac{\partial q}{\partial t} = k_a C(q_m - q) - k_d q \tag{52}$$

Fig. 2. A typical S-shape breakthrough curve. The corresponding position of the mass transfer zone in the column is shown on top of the curve. (C_b = breakthrough concentration; C_0 = feed concentration; t_b = breakthrough time; t_s = saturation time) [269].

where q_m is the monolayer capacity of the adsorbent in mg/g.

Thomas [244] gave an exact solution to Eq. (50) by substituting Eq. (52) into Eq. (50) and neglecting axial dispersion ($D_L = 0$, plug flow). Despite the analytical expression for the breakthrough curve, the mathematics involved is complex and cumbersome. Furthermore, Langmuir kinetics and zero axial dispersion do not reflect most real adsorption systems. As a result, many numerical methods have been developed to solve Eq. (50). Although powerful computers are available, these rigorous models involve many interdependent kinetic/transport parameters that need to be known before simulation [245]. The trial-and-error fitting of simulated results to experimental curves is required to confirm the truthfulness of these parameters. Hence, simplified models with fewer parameters that retain accuracy without the need for a complex numerical solution are desirable in the environmental adsorption studies [246]. Some common breakthrough models are presented in Section 6.2. In most cases, C is given as a function of t at fixed height Z, the value of which is the bed length.

6.2. Kinetic models for dynamic adsorption

6.2.1. Bohart–Adams model and Yoon–Nelson model
6.2.1.1. Bohart–Adams model. The fixed bed model proposed by Bohart and Adams is perhaps the most well-known [247]. The Bohart–Adams model is a simplified solution for the rigorous mass balance equation that assumes (i) a negligible axial dispersion and (ii) a rate of the following form, which is equivalent to a rectangular isotherm.

$$\frac{\partial q}{\partial t} = k_{BA} C(q_e - q) \tag{53}$$

For a rectangular isotherm, equilibrium q_e is independent of the solution concentration, that is, $q_e = q_0 =$ constant for all adsorptive concentration. The linearized form of the Bohart–Adams equation is written as

$$ln\left(\frac{C_0}{C} - 1\right) = \frac{k_{BA} N_0 Z}{u} - k_{BA} C_0 t \tag{54}$$

where $k_{BA} =$ Bohart–Adams rate constant ($cm^3/(mg \cdot min)$), $N_0 =$ adsorption capacity per unit volume of sorbent bed (mg/cm^3), and $u =$ superficial velocity (cm/min). Plotting $ln(C_0/C - 1)$ versus t gives $-k_{BA} C_0$ as slope and $k_{BA} N_0 Z/u$ as intercept. In the literature of liquid adsorption, the Bohart–Adams model often takes a limiting form, as given by Eq. (55), valid for $C/C_0 \ll 1$.

$$\ln \frac{C_0}{C} = \frac{k_T q_0 m}{Q} - k_T C_0 t \tag{55}$$

An alternative form of the Bohart–Adams model [Eq. (54)] is Eq. (56), which is often incorrectly referred to as the Thomas model.

$$ln\left(\frac{C_0}{C} - 1\right) = \frac{k_T q_0 m}{Q} - k_T C_0 t \tag{56}$$

where $k_T =$ Thomas rate constant ($cm^3/(mg \cdot min)$), $q_0 =$ maximum solid phase at saturation (mg/g), and $m =$ adsorbent mass in column (g).

Eqs. (54) and (56) are mathematically equivalent [248]. The misattribution of Eq. (56) to Thomas has become almost a convention that is difficult to redress. The Thomas model should refer to the analytical solution of Eqs. (50) and (52) to set the attribution right [248].

This paper seeks to name the model equations correctly while maintaining consistency with literature. Careful naming has to be adhered to for this apparent awkwardness to be addressed. In this paper, incorrect but widely adopted naming will be enclosed in quotation marks. For example, Eq. (54) shall be called Bohart–Adams model, while Eq. (55) shall be called 'Bohart–Adams model.' Eq. (56) will be referred to as 'Thomas model.' The analytical solution for Eqs. (50) and (52) is rightfully named the Thomas model.

The assumption of an irreversible, rectangular isotherm does not work for most adsorption systems, thereby resulting in the
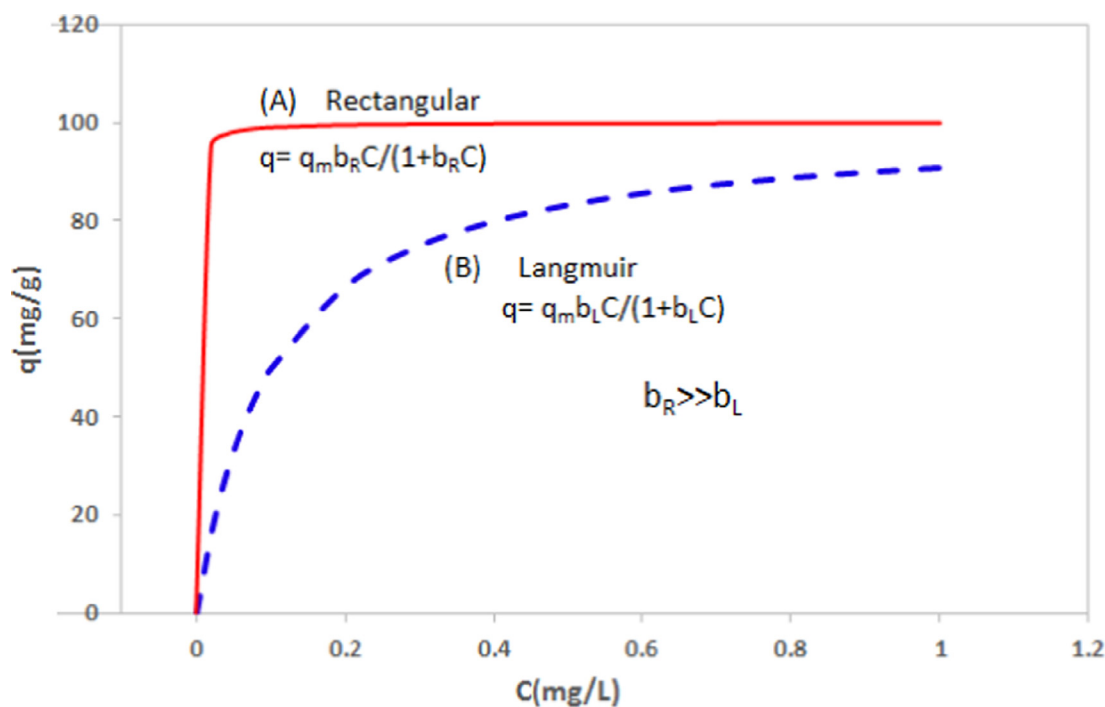
Fig. 3. Comparison of rectangular (A) and Langmuir (B) isotherms (b_r and b_L are Langmuir constants in l/mg) [248].

limited applicability of the Bohart–Adams equation. In fact, the Bohart–Adams model is a limiting case for the Thomas model when the Langmuir isotherm of the latter is highly favorable (i.e., large Langmuir constant, b_L or b_R in Fig. 3) [248]. Rectangular and Langmuir isotherms are shown in Fig. 3. The Thomas model, which assumes Langmuir adsorption characteristics [Eq. (52)], is more realistic and provides a better fit to breakthrough data.

6.2.1.2. Yoon–Nelson model

Yoon and Nelson proposed a simpler model to predict respirator cartridge service life [249]. The linearized form is

$$ln\left(\frac{C}{C_0 - C}\right) = k_{YN}(t - \tau) \tag{57}$$

where k_{YN} is the rate constant (min^{-1}), and τ is the time (min) required for 50% adsorbate breakthrough. Both parameters can be estimated through a $ln(\frac{C}{C_0 - C})$ versus t plot. The distinctive feature is that no detailed information about the adsorbent particles and bed properties is required for modeling purpose. This concise model has shown better fit than the Bohart–Adams model in many situations, e.g., adsorption of Cd(II) on leaf powder [250], pharmaceutical adsorption on pillared clay [251], and cephalexin adsorption by activated carbon [129]. The adsorption capacities calculated from the breakthrough curve and from the Yoon–Nelson model show a good match in Cd(II) adsorption [250].

The Yoon–Nelson model is mathematically equivalent to the Bohart–Adams model. The Yoon–Nelson parameters can be converted to Bohart–Adams parameters, and vice versa [252]. The Thomas model is different from the Yoon–Nelson and Bohart–Adams models in that the Thomas model is an exact solution that has no linearized form.

6.2.1.3. General equation for Bohart–Adams model, 'Thomas model,' and Yoon–Nelson model.
The Bohart–Adams model, 'Thomas model,' and the Yoon–Nelson model are the three most popular models for fixed bed modeling. They conform to a general equation form [252].

Nonlinear form: $\dfrac{C}{C_0} = \dfrac{1}{1 + \exp(a - bt)}$ (58)

Linearized form: $ln\left(\dfrac{C_0}{C} - 1\right) = a - bt$ (59)

For Bohart–Adams model, $a = k_{BA}N_0Z/u$ and $b = k_{BA}C_0$. For the 'Thomas model,' $a = k_T q_0 m/Q$ and $b = k_T C_0$. For the Yoon–Nelson model, $a = \tau\ k_{YN}$ and $b = k_{YN}$.

6.2.2. Bed depth service time (BDST)

In another model proposed by Hutchins [253], the BDST model takes the following form:

$$C_0 t = \frac{q_0 m}{Q} - \frac{1}{k_{BA}} ln\left(\frac{C_0}{C} - 1\right) \tag{60}$$

This form is actually a rearranged form of the linear Bohart–Adams equation. Therefore, comparing its adequacy of fit against the Bohart–Adams model using the same set of experimental data is meaningless. The BDST and Bohart–Adams model parameters are inter-convertible.

6.2.3. Clark model

Clark proposed a kinetic equation based on bed differential mass balance and Freundlich equilibrium behavior [254]. The linearized form is

$$ln\left(\left(\frac{C_0}{C}\right)^{n-1} - 1\right) = ln\ A - rt \tag{61}$$

where n is the Freundlich heterogeneity parameter, and

$$A = exp\left(\frac{k_C N_0 Z}{u}\right) \tag{61a}$$

$$r = k_C C_0. \tag{61b}$$

where k_C = Clark adsorption rate coefficient [cm^3/(mg•min)].

The Clark equation successfully modeled the breakthrough curves of lead ion adsorption onto a natural zeolite [255] and pharmaceutical adsorption on pillared clay [251]. It was able to predict the breakthrough behavior at various bed lengths [255].

6.2.4. Wolborska model

The Wolborska model was proposed to describe the breakthrough curve at the low concentration range [256]. The linearized form is

$$ln\left(\frac{C}{C_0}\right) = \frac{\beta_a C_0}{N_0}t - \frac{\beta_a Z}{u} \tag{62}$$

where C_0 = feed concentration of adsorptive (mg/l), β_a = kinetic coefficient for external mass transfer (min^{-1}), N_0 = maximum amount adsorbed per unit volume of adsorbent (mg/l), and u = superficial velocity (cm/min).

From a $ln(\frac{C}{C_0})$ versus t plot, N_0 and β_a can be determined from the slope and intercept, respectively. This model becomes a Bohart–Adams model if $k_{BA} = \beta_a/N_0$. In many instances, this model provides good fit only to the initial portion of the breakthrough curve [257-259]. It has provided good fit for $ln(C/C_0) < -2$ in the case of copper(II) removal by cation exchange resin [259] and methylene blue removal by melon peel [260].

6.2.5. Modified dose response (MDR) model

Yan et al. [261] proposed the MDR model, the integrated form of which is

$$\frac{C}{C_0} = 1 - \frac{1}{1 + \left(\frac{C_0 Q t}{q_0 m}\right)^a} \tag{63}$$

where C_0 = bed inlet concentration of adsorptive (mg/l), m = adsorbent dose (g), Q = feed flowrate (l/min), q_0 = maximum adsorption capacity of bed (mg/g), and a = model constant.

Applications of the modified dose response model were carried out by Zeinali et al. [262] and Singh et al. [263].

7. Modeling works on fixed bed adsorption systems

Column studies that attempt to model the breakthrough curves are relatively scarce. Table 7 shows some fixed bed modeling studies on the separation of pollutants from aqueous media. The effects of influent adsorptive concentrations, flowrate, and bed height are well studied. Generally, the column saturation capacity increases with influent concentration but decreases with increasing flowrate [264,265].

'Thomas model' and Yoon–Nelson model provide equally good fit as they should because of their mathematically equivalent forms. Likewise, 'Bohart–Adams' and Wolborska show similar suitability at the initial period of adsorption [257,258,263,264] because of their similar mathematical forms. As expected, 'Bohart–Adams model' fits the initial kinetics because it is a limiting form for $C/C_0 \ll 1$. The Wolborska model is similar in form to the 'Bohart–Adams model' and hence shows a similar fit.

In [203], the Clark model was able to track the phenol uptake onto chemically modified resin. The fitted n was 2.451, which is close to the n value (2.060) given by the Freundlich isotherm, thereby indicating the suitability of the Clark model.

Although some models, like the 'Thomas model' and Clark model, have some theoretical origins, they are in oversimplified form and applied much like empirical models are. One prominent drawback of an empirical model is its limited range of validity. It is usually valid only within the range of operating conditions under which it is fitted. Extrapolation of the model to extended operating range does not promise good results. How the fitted model will respond when operating conditions change is not well studied. The parameter in the model that should be changed to reflect the possible deviation in kinetic behavior is also unclear. Often, a refitting is warranted under such situations to obtain a new set of model parameters. The Clark model is able to predict the breakthrough curves recorded for shorter beds [255].

Some issues pertinent to fixed bed kinetics modeling are the following:

(i) Experimental bed capacity is not provided. Only predicted capacities can be inferred from the fitted parameters of the model. The predicted capacities from different models have no experimental values to compare with. A comparison with the Langmuir isotherm monolayer capacity is unreliable. Models are differentiated based solely on R^2 or statistical error functions.

(ii) Experimental bed capacity is provided, but batch adsorption capacity is not. The fixed bed performance has no reference for comparison.

Modeling should be carried out only for a properly characterized fixed bed system. The modeling results would be well worth the effort if the column performs well and in a repeatable manner.

8. Concluding remarks and outlook

A number of theoretical interpretations have been proposed for PFO and PSO models, which are the most common empirical models in liquid adsorption. These two models are supposed to fit chemical reaction controlled kinetics. However, theoretical interpretations have revealed that successful fitting of these pseudo models alone is no guarantee of chemisorption control. Diffusion or combined diffusion–reaction control is also possible from a theoretical perspective. No single theoretical background can explain the kinetics in each and every case fitted by the PFO or PSO model. Two reasons are possible: (i) these theoretical derivations are based on certain assumptions or experimental conditions and hence have a restricted range of validity; (ii) PFO or PSO is a combination of several models with multiple controlling mechanisms that are not captured by a single interpretation. More often than not, these interpretations involve parameters (e.g., surface adsorption and desorption constants) that are difficult to obtain from experiments. Determining the values of these physical parameters is not straightforward, thereby limiting their potential widespread applications.

Pseudo-second-order model can describe all adsorption systems virtually, asserting its superiority in curve fitting. Numerous environmental studies have adopted a lumped approach to kinetics modeling using PSO. Despite the excellent curve fit, the obtained lumped rate constant has no clear kinetic significance because of unclear kinetic regime. Furthermore, these studies seldom seek to further understand the underlying adsorbent–adsorbate behavior. Two reasons are accountable for this lack of interest. First, these works focus on the novelty of adsorbent material rather than the kinetics. Second, relating to existing theoretical interpretations is difficult as the applicability range of these theories is not clearly defined nor experimentally proven. The pseudo-order models have value in their simplicity and ease of use for modeling and process simulation. The model rate constants can be made to bear certain physicochemical significance by the proper control of experimental conditions. With regard to model fitting, nonlinear regression should be preferred over linear regression to avoid the bias induced by linearization transformation.

From a design perspective, a lumped approach to kinetic modeling would suffice. However, a mechanistic (theoretical) model is preferred to understand the mechanism that controls the overall adsorption kinetics. Embedding the mechanism into a model would greatly enhance the predictive capability of the model and enable process simulation and optimization over a wide range of operating conditions, thereby saving experimental cost. However, solving mechanistic models of such complexity is computationally demanding and time consuming. Therefore, a balance between lumped and mechanistic approach of modeling is advised for prac-

ARTICLE IN PRESS

Table 7
Selected works on fixed bed modeling for the removal of various pollutants from water.

Adsorbate	Adsorbent	Temperature (°C)	Influent adsorptive concentration, C_0(mg/l, except otherwise stated)	Influent flowrate, ml/min	Experimental bed saturation capacity, q_{exp}(mg/g, except stated otherwise)	Candidate model (the best fit model(s) in bold)	Regression type	Discrimination	Reference
Pb	Natural zeolite clinoptilolite	25	2.513 mmol/l	1	0.574 mmol/g	**Clark**	nonlinear	R^2,RMSE	[255]
Cu; Pb	Spirogyra biomass granules	25	50	0.6	26.7; 56.1	**'Thomas', Yoon–Nelson, MDR,** 'Bohart-Adams', Wolborska	nonlinear	R^2	[263]
Phenol	Nmethylacetamide-modified hypercrosslinked resin	–	501.2	1	199.8	**'Thomas', Clark**	nonlinear	–	[203]
Atenolol; Isoproturon	Granular activated carbon (GAC)	25	500 μg/l; 150 μg/l	1.5; 1.5	34.44; 19.5	BDST, **'Thomas'**, Wolborska, **Yoon-Nelson**, Clark	nonlinear	RMSE, MPSD	[266]
Caffeine; Diclofenac	GAC	25	15; 10	2; 3	255.4; 182.9	**BDST**	linear	–	[267]
Dichloromethane; Toluene	GAC	30	12,380; 294	20; 90	29.48 mmol/g; 1.94 mmol/g	'Thomas', Yoon–Nelson, **Yan**	–	R^2	[262]
Chemical oxygen demand (COD) and color in cotton textile wastewater	Rattan AC	28	251.65(COD); 486.87 Pt/Co(color)	10	73.23; 100.15 Pt/Co	**'Thomas', 'Bohart-Adams', Yoon–Nelson**	linear	R^2, ARE	[264]
Nitrate	Aminated polystyrene resin	25	200	1	317.83	**'Thomas', Yoon–Nelson, Bohart-Adams**	nonlinear	R^2	[268]
Methylene Blue	Pine cone biomass	25	70	12	42.49	**'Thomas', BDST, Yoon–Nelson**	nonlinear	R^2	[265]
Salicylic acid; Carbamazepine; Caffeine	Metal modified bentonite	25	14	2	4.964; 4.592; 3.469	Yoon Nelson, Clark, **MDR**	–	ARE,MPSD	[251]
Mercury	Chemical-modified rice straw	–	50	4	205.05	'Bohart-Adams', **'Thomas'**, BDST, **Yoon–Nelson**	linear	R^2	[76]
Cephalexin	Walnut shell AC	30	100	6	139.98	'Bohart-Adams', **'Thomas', Yoon-Nelson**	linear	SSE,R^2,R^2_{adj}	[129]
Orange G	Basic anion exchange resin	–	750	1.13	1386	**'Thomas', Yoon–Nelson, Wolborska**	nonlinear	R^2	[257]
Phenol	Modified rice husk	–	500	22/3	1341.46	Bohart–Adams, **'Thomas', Yoon–Nelson**, Wolborska	linear	R^2,ARE	[258]

tical design purposes. A practical model should have an empirical form with physicochemically sound parameters.

The adsorption operation is complex from a theoretical perspective. The as-measured total uptake rate can be contributed by a single adsorption route or multiple parallel adsorption routes. Each route is controlled by different mechanisms at different adsorption times. Tracking these changes in all adsorption systems is virtually impossible for the whole period by using a universal model. An immediately viable approach would be to divide the adsorption course into several periods and model each period with a theoretically sound model to probe into such complex mechanism. A composite model can then be constructed for the entire process on the basis of these models. Starting with simple models that consider only a single rate-controlling step in each period before more complex models are engaged is always wise. Considering the complexities and restriction of the theoretical models, the empirical or at best 'rationalized' empirical models, such as the pseudo-order models, shall remain relevant and attractive in the modeling of liquid adsorption kinetics for practical purposes.

References

[1] Kyzas GZ, Kostoglou M, Lazaridis NK, Lambropoulou DA, Bikiaris DN. Environmental friendly technology for the removal of pharmaceutical contaminants from wastewaters using modified chitosan adsorbents. Chem Eng J 2013;222:248–58.

[2] Li X, Ying G-G, Zhao J-L, Chen Z-F, Lai H-J, Su H-C. 4-Nonylphenol, bisphenol-A and triclosan levels in human urine of children and students in China, and the effects of drinking these bottled materials on the levels. Environ Int 2013;52:81–6.

[3] Nassef M, Matsumoto S, Seki M, et al. Acute effects of triclosan, diclofenac and carbamazepine on feeding performance of Japanese medaka fish (Oryzias latipes). Chemosphere 2010;80:1095–100.

[4] Raval NP, Shah PU, Shah NK. Adsorptive removal of nickel(II) ions from aqueous environment: a review. J Environ Manag 2016;179:1–20.

[5] Du Z, Deng S, Bei Y, Huang Q, Wang B, Huang J, et al. Adsorption behavior and mechanism of perfluorinated compounds on various adsorbents–a review. J Hazard Mater 2014;274:443–54.

[6] Hasan Z, Jhung SH. Removal of hazardous organics from water using metal-organic frameworks (MOFs): plausible mechanisms for selective adsorptions. J Hazard Mater 2015;283:329–39.

[7] Kyzas G, Kostoglou M. Green adsorbents for wastewaters: a critical review. Materials 2014;7:333–64.

[8] Ahmed MB, Zhou JL, Ngo HH, Guo W. Adsorptive removal of antibiotics from water and wastewater: progress and challenges. Sci Total Environ 2015;532:112–26.

[9] Adegoke KA, Bello OS. Dye sequestration using agricultural wastes as adsorbents. Water Resour Ind 2015;12:8–24.

[10] Alberti G, Amendola V, Pesavento M, Biesuz R. Beyond the synthesis of novel solid phases: review on modelling of sorption phenomena. Coord Chem Rev 2012;256:28–45.

[11] Plazinski W, Rudzinski W, Plazinska A. Theoretical models of sorption kinetics including a surface reaction mechanism: a review. Adv Colloid Interface Sci 2009;152:2–13.

[12] Liu Y, Wang Z-W. Uncertainty of preset-order kinetic equations in description of biosorption data. Bioresour Technol 2008;99:3309–12.

[13] Özer A. Removal of Pb(II) ions from aqueous solutions by sulphuric acid-treated wheat bran. J Hazard Mater 2007;141:753–61.

[14] Lin C-I, Wang L-H. Rate equations and isotherms for two adsorption models. J Chin Inst Chem Eng 2008;39:579–85.

[15] Liu Y, Yang S-F, Xu H, Woon K-H, Lin Y-M, Tay J-H. Biosorption kinetics of cadmium(II) on aerobic granular sludge. Process Biochem 2003;38:997–1001.

[16] Ho YS. Review of second-order models for adsorption systems. J Hazard Mater 2006;136:681–9.

[17] Liu Y, Liu YJ. Biosorption isotherms, kinetics and thermodynamics. Sep Purif Technol 2008;61:229–42.

[18] Ho YS, Ng JCY, McKay G. Kinetics of pollutant sorption by biosorbents: review. Sep Purif Methods 2000;29:189–232.

[19] Amanullah M, Viswanathan S, Farooq S. Equilibrium, kinetics, and column dynamics of methyl ethyl ketone biodegradation. Ind Eng Chem Res 2000;39:3387–96.

[20] Plazinski W, Rudzinski W. A novel two-resistance model for description of the adsorption kinetics onto porous particles. Langmuir 2010;26:802–8.

[21] Rudzinski W, Plazinski W. Kinetics of dyes adsorption at the solid-solution interfaces: a theoretical description based on the two-step kinetic model. Environ Sci Technol 2008;42:2470–5.

[22] Keller JU, Staudt R. Gas adsorption equilibria: experimental methods and adsorption isotherms. New York: Springer; 2005.

[23] Ruthven DM. Principles of adsorption and adsorption processes. New York: Wiley; 1984.

[24] Vithanage M, Mayakaduwa SS, Herath I, Ok YS, Mohan D. Kinetics, thermodynamics and mechanistic studies of carbofuran removal using biochars from tea waste and rice husks. Chemosphere 2016;150:781–9.

[25] Zhou L, Pan S, Chen X, Zhao Y, Zou B, Jin M. Kinetics and thermodynamics studies of pentachlorophenol adsorption on covalently functionalized Fe_3O_4@SiO_2–MWCNTs core–shell magnetic microspheres. Chem Eng J 2014;257:10–19.

[26] Kara M, Yuzer H, Sabah E, Celik MS. Adsorption of cobalt from aqueous solutions onto sepiolite. Water Res 2003;37:224–32.

[27] Foo KY, Hameed BH. Insights into the modeling of adsorption isotherm systems. Chem Eng J 2010;156:2–10.

[28] Slimani R, Anouzla A, Abrouki Y, et al. Removal of a cationic dye -Methylene Blue- from aqueous media by the use of animal bone meal as a new low cost adsorbent. J Mater Environ Sci 2011;2:77–87.

[29] Regti A, Laamari MR, Stiriba S-E, El Haddad M. Use of response factorial design for process optimization of basic dye adsorption onto activated carbon derived from Persea species. Microchem J 2017;130:129–36.

[30] Froment GF. Model discrimination and parameter estimation in heterogeneous catalysis. AIChE J 1975;21:1041–57.

[31] Lagergren S. About the theory of so-called adsorption of soluble substances. Kungliga Svenska Vetenskapsakademiens 1898;4:1–39 Band 24.

[32] Chinoune K, Bentaleb K, Bouberka Z, Nadim A, Maschke U. Adsorption of reactive dyes from aqueous solution by dirty bentonite. Appl Clay Sci 2016;123:64–75.

[33] Naushad M, Alothman ZA, Inamuddin Javadian H. Removal of Pb(II) from aqueous solution using ethylene diamine tetra acetic acid-Zr(IV) iodate composite cation exchanger: kinetics, isotherms and thermodynamic studies. J Ind Eng Chem 2015;25:35–41.

[34] Pandey PK, Sharma SK, Sambi SS. Removal of lead(II) from waste water on zeolite-NaX. J Environ Chem Eng 2015;3:2604–10.

[35] Zarezadeh-Mehrizi M, Badiei A. Highly efficient removal of basic blue 41 with nanoporous silica. Water Resour Ind 2014;5:49–57.

[36] Yousef RI, El-Eswed B, AaH Al-Muhtaseb. Adsorption characteristics of natural zeolites as solid adsorbents for phenol removal from aqueous solutions: kinetics, mechanism, and thermodynamics studies. Chem Eng J 2011;171:1143–1149.

[37] Biswas S, Mishra U. Effective remediation of lead ions from aqueous solution by chemically carbonized rubber wood sawdust: equilibrium, kinetics, and thermodynamic study. J Chem 2015;2015:1–8.

[38] Vincent T, Taulemesse J-M, Dauvergne A, Chanut T, Testa F, Guibal E. Thallium(I) sorption using Prussian blue immobilized in alginate capsules. Carbohydr Polym 2014;99:517–26.

[39] Rudzinski W, Plazinski W. Studies of the kinetics of solute adsorption at solid/solution interfaces: on the possibility of distinguishing between the diffusional and the surface reaction kinetic models by studying the pseudo–first-order kinetics. J Phys Chem C 2007;111:15100–10.

[40] Ho YS, McKay G. The sorption of lead(II) ions on peat. Water Res 1999;33:578–84.

[41] McKay G, Ho YS, Ng JCY. Biosorption of copper from waste waters: a review. Sep Purif Methods 1999;28:87–125.

[42] Tien C. Remarks on adsorption manuscripts revised and declined: an editorial. J Hazard Mater 2008;150:2–3.

[43] El-Khaiary MI, Malash GF. Common data analysis errors in batch adsorption studies. Hydrometallurgy 2011;105:314–20.

[44] Douven S, Paez CA, Gommes CJ. The range of validity of sorption kinetic models. J Colloid Interface Sci 2015;448:437–50.

[45] Yang X, Al-Duri B. Kinetic modeling of liquid-phase adsorption of reactive dyes on activated carbon. J Colloid Interface Sci 2005;287:25–34.

[46] Azizian S, Bashiri H. Adsorption kinetics at the solid/solution interface: statistical rate theory at initial times of adsorption and close to equilibrium. Langmuir 2008;24:11669–76.

[47] Rudzinski W, Plazinski W. Kinetics of solute adsorption at solid/aqueous interfaces: searching for the theoretical background of the modified pseudo–first-order kinetic equation. Langmuir 2008;24:5393–9.

[48] Ho YS, McKay G. Pseudo-second order model for sorption processes. Process Biochem 1999;34:451–65.

[49] Ho YS. Second-order kinetic model for the sorption of cadmium onto tree fern: a comparison of linear and non-linear methods. Water Res 2006;40:119–25.

[50] Setiabudi HD, Jusoh R, Suhaimi SFRM, Masrur SF. Adsorption of methylene blue onto oil palm (Elaeis guineensis) leaves: process optimization, isotherm, kinetics and thermodynamic studies. J Taiwan Inst Chem Eng 2016;63:363–70.

[51] Nazari M, Halladj R. Adsorptive removal of fluoride ions from aqueous solution by using sonochemically synthesized nanomagnesia/alumina adsorbents: an experimental and modeling study. J Taiwan Inst Chem Eng 2014;45:2518–25.

[52] Franca AS, Oliveira LS, Ferreira ME. Kinetics and equilibrium studies of methylene blue adsorption by spent coffee grounds. Desalination 2009;249:267–72.

[53] El Haddad M, Slimani R, Mamouni R, ElAntri S, Lazar S. Removal of two textile dyes from aqueous solutions onto calcined bones. J Assoc Arab Univ Basic Appl Sci 2013;14:51–9.

[54] Allen SJ, Gan Q, Matthews R, Johnson PA. Kinetic modeling of the adsorption of basic dyes by kudzu. J Colloid Interface Sci 2005;286:101–9.

[55] Febrianto J, Kosasih AN, Sunarso J, Ju Y-H, Indraswati N, Ismadji S. Equilibrium and kinetic studies in adsorption of heavy metals using biosorbent: a summary of recent studies. J Hazard Mater 2009;162:616–45.

[56] Namasivayam C, Sangeetha D. Application of coconut coir pith for the removal of sulfate and other anions from water. Desalination 2008;219:1–13.

[57] Fogler HS. Elements of chemical reaction engineering, Upper Saddle River, NJ: Prentice Hall PTR; 2006. 4th ed.

[58] Froment GF, Bischoff KB, De Wilde J. Chemical reactor analysis and design, Hoboken, N.J.: Wiley; 2011. 3rd ed.

[59] Lin KY, Liu YT, Chen SY. Adsorption of fluoride to UiO-66-NH$_2$ in water: stability, kinetic, isotherm and thermodynamic studies. J Colloid Interface Sci 2016;461:79–87.

[60] Song S-T, Saman N, Johari K, Mat H. Removal of Hg(II) from aqueous solution by adsorption using raw and chemically modified rice straw as novel adsorbents. Ind Eng Chem Res 2013;52:13092–101.

[61] Arnold FH, Blanch HW. Analytical affinity chromatography. II. Rate theory and the measurement of biological binding kinetics. J Chromatogr A 1986;355:13–27.

[62] Boyer PM, Hsu JT. Effects of ligand concentration on protein adsorption in dye-ligand adsorbents. Chem Eng Sci 1992;47:241–51.

[63] Perego C, Peratello S. Experimental methods in catalytic kinetics. Catal Today 1999;52:133–45.

[64] Azizian S. Kinetic models of sorption: a theoretical analysis. J Colloid Interface Sci 2004;276:47–52.

[65] Duran C, Ozdes D, Gundogdu A, Senturk HB. Kinetics and isotherm analysis of basic dyes adsorption onto almond shell (Prunus dulcis) as a low cost adsorbent. J Chem Eng Data 2011;56:2136–47.

[66] Li XM, Zheng W, Wang DB, et al. Removal of Pb (II) from aqueous solutions by adsorption onto modified areca waste: kinetic and thermodynamic studies. Desalination 2010;258:148–53.

[67] Njoku VO, Islam MA, Asif M, Hameed BH. Utilization of sky fruit husk agricultural waste to produce high quality activated carbon for the herbicide bentazon adsorption. Chem Eng J 2014;251:183–91.

[68] Miyake Y, Ishida H, Tanaka S, Kolev SD. Theoretical analysis of the pseudo-second order kinetic model of adsorption. Application to the adsorption of Ag(I) to mesoporous silica microspheres functionalized with thiol groups. Chem Eng J 2013;218:350–7.

[69] Plazinski W. Applicability of the film-diffusion model for description of the adsorption kinetics at the solid/solution interfaces. Appl Surf Sci 2010;256:5157–63.

[70] Plazinski W, Dziuba J, Rudzinski W. Modeling of sorption kinetics: the pseudo-second order equation and the sorbate intraparticle diffusivity. Adsorption 2013;19:1055–64.

[71] Acemioğlu B. Batch kinetic study of sorption of methylene blue by perlite. Chem Eng J 2005;106:73–81.

[72] Aroua MK, Leong SPP, Teo LY, Yin CY, Daud WMAW. Real-time determination of kinetics of adsorption of lead(II) onto palm shell-based activated carbon using ion selective electrode. Bioresour Technol 2008;99:5786–92.

[73] Azizian S, Fallah RN. A new empirical rate equation for adsorption kinetics at solid/solution interface. Appl Surf Sci 2010;256:5153–6.

[74] Cooney DO. Adsorption design for wastewater treatment. Boca Raton, Fl: Lewis Publishers; 1999.

[75] Özacar M, Şengýl IA. Two-stage batch sorber design using second-order kinetic model for the sorption of metal complex dyes onto pine sawdust. Biochem Eng J 2004;21:39–45.

[76] Song S-T, Hau Y-F, Saman N, Johari K, Cheu S-C, Kong H, et al. Process analysis of mercury adsorption onto chemically modified rice straw in a fixed-bed adsorber. J Environ Chem Eng 2016;4:1685–97.

[77] Kumar U, Bandyopadhyay M. Fixed bed column study for Cd(II) removal from wastewater using treated rice husk. J Hazard Mater 2006;129:253–9.

[78] Roginsky S, Zeldovich YB. The catalytic oxidation of carbon monoxide on manganese dioxide. Acta Phys Chem USSR 1934;1:554.

[79] Acevedo B, Barriocanal C, Lupul I, Gryglewicz G. Properties and performance of mesoporous activated carbons from scrap tyres, bituminous wastes and coal. Fuel 2015;151:83–90.

[80] Teng H, Hsieh CT. Activation energy for oxygen chemisorption on carbon at low temperatures. Ind Eng Chem Res 1999;38:292–7.

[81] Rudzinski W, Panczyk T. Surface heterogeneity effects on adsorption equilibria and kinetics: rationalizations of the Elovich equation. In: Schwarz JA, Contescu CI, editors. Surfaces of nanoparticles and porous materials. New York: Marcel Dekker; 1999. p. 355–90.

[82] Piasecki W, Rudziński W. Application of the statistical rate theory of interfacial transport to investigate the kinetics of divalent metal ion adsorption onto the energetically heterogeneous surfaces of oxides and activated carbons. Appl Surf Sci 2007;253:5814–17.

[83] Largitte L, Pasquier R. A review of the kinetics adsorption models and their application to the adsorption of lead by an activated carbon. Chem Eng Res Des 2016;109:495–504.

[84] Elkady MF, Ibrahim AM, El-Latif MMA. Assessment of the adsorption kinetics, equilibrium and thermodynamic for the potential removal of reactive red dye using eggshell biocomposite beads. Desalination 2011;278:412–23.

[85] Shehata FA, Attallah MF, Borai EH, Hilal MA, Abo-Aly MM. Sorption reaction mechanism of some hazardous radionuclides from mixed waste by impregnated crown ether onto polymeric resin. Appl Radiat Isot 2010;68:239–49.

[86] Baral SS, Das SN, Rath P. Hexavalent chromium removal from aqueous solution by adsorption on treated sawdust. Biochem Eng J 2006;31:216–22.

[87] Debnath S, Ghosh UC. Kinetics, isotherm and thermodynamics for Cr(III) and Cr(VI) adsorption from aqueous solutions by crystalline hydrous titanium oxide. J Chem Thermodyn 2008;40:67–77.

[88] Hu J, Chen C, Zhu X, Wang X. Removal of chromium from aqueous solution by using oxidized multiwalled carbon nanotubes. J Hazard Mater 2009;162:1542–50.

[89] Haerifar M, Azizian S. Fractal-like adsorption kinetics at the solid/solution interface. J Phys Chem C 2012;116:13111–19.

[90] Cestari AR, Vieira EFS, Lopes ECN, da Silva RG. Kinetics and equilibrium parameters of Hg(II) adsorption on silica–dithizone. J Colloid Interface Sci 2004;272:271–6.

[91] Lopes ECN, dos Anjos FSC, Vieira EFS, Cestari AR. An alternative Avrami equation to evaluate kinetic parameters of the interaction of Hg(II) with thin chitosan membranes. J Colloid Interface Sci 2003;263:542–7.

[92] Vaghetti JC, Lima EC, Royer B, da Cunha BM, Cardoso NF, Brasil JL, et al. Pecan nutshell as biosorbent to remove Cu(II), Mn(II) and Pb(II) from aqueous solutions. J Hazard Mater 2009;162:270–80.

[93] Alencar WS, Lima EC, Royer B, dos Santos BD, Calvete T, da Silva EA, et al. Application of aqai stalks as biosorbents for the removal of the dye Procion Blue MX-R from aqueous solution. Sep Sci Technol 2012;47:513–26.

[94] Liu Y, Shen L. A general rate law equation for biosorption. Biochem Eng J 2008;38:390–4.

[95] Saucier C, Adebayo MA, Lima EC, et al. Microwave-assisted activated carbon from cocoa shell as adsorbent for removal of sodium diclofenac and nimesulide from aqueous effluents. J Hazard Mater 2015;289:18–27.

[96] Ribas MC, Adebayo MA, Prola LDT, et al. Comparison of a homemade cocoa shell activated carbon with commercial activated carbon for the removal of reactive violet 5 dye from aqueous solutions. Chem Eng J 2014;248:315–26.

[97] Heydari-Gorji A, Sayari A. CO$_2$ capture on polyethylenimine-impregnated hydrophobic mesoporous silica: experimental and kinetic modeling. Chem Eng J 2011;173:72–9.

[98] Brouers F, Sotolongo-Costa O. Generalized fractal kinetics in complex systems (application to biophysics and biotechnology). Phys A: Stat Mech Appl 2006;368:165–75.

[99] Cussler EL. Diffusion. Mass transfer in fluid systems, New York: Cambridge University Press; 2009. 3rd ed.

[100] Crank J. The mathematics of diffusion. London: Oxford University Press; 1956.

[101] Boyd GE, Adamson AW, Myers LS. The exchange adsorption of ions from aqueous solutions by organic zeolites. II. Kinet J Am Chem Soc 1947;69:2836–48.

[102] Hameed BH, El-Khaiary MI. Batch removal of malachite green from aqueous solutions by adsorption on oil palm trunk fibre: equilibrium isotherms and kinetic studies. J Hazard Mater 2008;154:237–44.

[103] Vermeulen T. Theory for irreversible and constant-pattern solid diffusion. Ind Eng Chem 1953;45:1664–70.

[104] Balsamo M, Montagnaro F. Fractal-like Vermeulen kinetic equation for the description of diffusion-controlled adsorption dynamics. J Phys Chem C 2015;119:8781–5.

[105] Elkady MF, Abu-Saied MA, Abdel Rahman AM, Soliman EA, Elzatahry AA, Elsayed Yossef M, et al. Nano-sulphonated poly (glycidyl methacrylate) cations exchanger for cadmium ions removal: effects of operating parameters. Desalination 2011;279:152–62.

[106] Sivashankar R, Sathya AB, Vasantharaj K, Sivasubramanian V. Reduction of azo dye from aqueous solution using acid treated aquatic macrophytes. J Environ Nanotechnol 2014;3:50–61.

[107] McKay G, Otterburn MS, Aga JA. Fuller's earth and fired clay as adsorbents for dyestuffs. Water, Air, Soil Pollut 1985;24:307–22.

[108] Vergili I, Soltobaeva G, Kaya Y, Gönder ZB, Çavuş S, Gürdağ G. Study of the removal of Pb(II) using a weak acidic cation resin: kinetics, thermodynamics, equilibrium, and breakthrough curves. Ind Eng Chem Res 2013;52:9227–38.

[109] Urano K, Tachikawa H. Process development for removal and recovery of phosphorus from wastewater by a new adsorbent. 2. Adsorption rates and breakthrough curves. Ind Eng Chem Res 1991;30:1897–9.

[110] Dizge N, Keskinler B, Barlas H. Sorption of Ni(II) ions from aqueous solution by Lewatit cation-exchange resin. J Hazard Mater 2009;167:915–26.

[111] Weber WJ, Morris JC. Kinetics of adsorption on carbon from solution. J Sanit Eng Div 1963;89:31–60.

[112] Nazari G, Abolghasemi H, Esmaieli M. Batch adsorption of cephalexin antibiotic from aqueous solution by walnut shell-based activated carbon. J Taiwan Inst Chem Eng 2016;58:357–65.

[113] Sarkar AK, Pal A, Ghorai S, Mandre NR, Pal S. Efficient removal of malachite green dye using biodegradable graft copolymer derived from amylopectin and poly(acrylic acid). Carbohydr Polym 2014;111:108–15.

[114] Víctor-Ortega MD, Ochando-Pulido JM, Martínez-Férez A. Phenols removal from industrial effluents through novel polymeric resins: kinetics and equilibrium studies. Sep Purif Technol 2016;160:136–44.

[115] Liu X, Zhang L. Removal of phosphate anions using the modified chitosan beads: adsorption kinetic, isotherm and mechanism studies. Powder Technol 2015;277:112–19.

[116] Ma X, Li L, Yang L, Su C, Wang K, Yuan S, et al. Adsorption of heavy metal ions using hierarchical CaCO$_3$-maltose meso/macroporous hybrid materials: adsorption isotherms and kinetic studies. J Hazard Mater 2012;209-210:467–77.

[117] Vázquez G, Mosquera O, Freire MS, Antorrena G, González-Álvarez J. Alkaline pre-treatment of waste chestnut shell from a food industry to enhance cadmium, copper, lead and zinc ions removal. Chem Eng J 2012;184:147–55.

[118] Chen Z, Zhang J, Fu J, Wang M, Wang X, Han R, et al. Adsorption of methylene blue onto poly(cyclotriphosphazene-co-4,4′-sulfonyldiphenol) nanotubes: kinetics, isotherm and thermodynamics analysis. J Hazard Mater 2014;273: 263–271.

[119] MdCE Pinto, Gonçalves RGL, dos Santos RMM, et al. Mesoporous carbon derived from a biopolymer and a clay: preparation, characterization and application for an organochlorine pesticide adsorption. Microporous Mesoporous Mater 2016;225:342–54.

[120] Rahman N, Haseen U. Equilibrium modeling, kinetic, and thermodynamic studies on adsorption of Pb(II) by a hybrid inorganic–organic material: poly-acrylamide zirconium(IV) iodate. Ind Eng Chem Res 2014;53:8198–207.

[121] Wu F-C, Tseng R-L, Juang R-S. Initial behavior of intraparticle diffusion model used in the description of adsorption kinetics. Chem Eng J 2009;153:1–8.

[122] Malash GF, El-Khaiary MI. Piecewise linear regression: a statistical method for the analysis of experimental adsorption data by the intraparticle-diffusion models. Chem Eng J 2010;163:256–63.

[123] Yang G, Chen H, Qin H, Feng Y. Amination of activated carbon for enhancing phenol adsorption: effect of nitrogen-containing functional groups. Appl Surf Sci 2014;293:299–305.

[124] Yang W, Ding P, Zhou L, Yu J, Chen X, Jiao F. Preparation of diamine modified mesoporous silica on multi-walled carbon nanotubes for the adsorption of heavy metals in aqueous solution. Appl Surf Sci 2013;282:38–45.

[125] McKay G, Otterburn MS, Sweeney AG. The removal of colour from effluent using various adsorbents—III. Silica: Rate Process Water Res 1980;14:15–20.

[126] Raji F, Pakizeh M. Kinetic and thermodynamic studies of Hg(II) adsorption onto MCM-41 modified by ZnCl$_2$. Appl Surf Sci 2014;301:568–75.

[127] Douven S, Paez CA, Gommes CJ. The range of validity of sorption kinetic models. J Colloid Interface Sci 2015;448:437–50.

[128] Rudzinski W, Plazinski W. Kinetics of solute adsorption at solid/solution interfaces: on the special features of the initial adsorption kinetics. Langmuir 2008;24:6738–44.

[129] Nazari G, Abolghasemi H, Esmaieli M, Sadeghi Pouya E. Aqueous phase adsorption of cephalexin by walnut shell-based activated carbon: a fixed-bed column study. Appl Surf Sci 2016;375:144–53.

[130] Aharoni C, Sideman S, Hoffer E. Adsorption of phosphate ions by collodion–coated alumina. J Chem Technol Biotechnol 1979;29:404–12.

[131] Gupta VK, Gupta B, Rastogi A, Agarwal S, Nayak A. Pesticides removal from waste water by activated carbon prepared from waste rubber tire. Water Res 2011;45:4047–55.

[132] Le Roux JD, Bryson AW, Young BD. Comparison of several kinetic models for the adsorption of gold cyanide onto activated carbon. J S Afr Inst Min Metall 1991;91:95–103.

[133] Haerifar M, Azizian S. Mixed surface reaction and diffusion-controlled kinetic model for adsorption at the solid/solution interface. J Phys Chem C 2013;117:8310–17.

[134] Marco-Brown JL, Areco MM, Torres Sánchez RM, dos Santos Afonso M. Adsorption of picloram herbicide on montmorillonite: kinetic and equilibrium studies. Colloids Surf A: Physicochem Eng Asp 2014;449:121–8.

[135] Wilczak A, Keinath TM. Kinetics of sorption and desorption of copper(II) and lead(II) on activated carbon. Water Environ Res 1993;65:238–44.

[136] Chiron N, Guilet R, Deydier E. Adsorption of Cu(II) and Pb(II) onto a grafted silica: isotherms and kinetic models. Water Res 2003;37:3079–86.

[137] Marczewski AW. Kinetics and equilibrium of adsorption of organic solutes on mesoporous carbons. Appl Surf Sci 2007;253:5818–26.

[138] Derylo-Marczewska A, Marczewski AW, Winter S, Sternik D. Studies of adsorption equilibria and kinetics in the systems: aqueous solution of dyes–mesoporous carbons. Appl Surf Sci 2010;256:5164–70.

[139] Li Z. Sorption kinetics of hexadecyltrimethylammonium on natural clinoptilolite. Langmuir 1999;15:6438–45.

[140] Shen XE, Shan XQ, Dong DM, Hua XY, Owens G. Kinetics and thermodynamics of sorption of nitroaromatic compounds to as-grown and oxidized multi-walled carbon nanotubes. J Colloid Interface Sci 2009;330:1–8.

[141] Achik J, Schiavon M, Jamet P. Study of carbofuran movement in soils part II-kinetics. Environ Int 1991;17:81–8.

[142] Cáceres L, Escudey M, Fuentes E, Báez ME. Modeling the sorption kinetic of metsulfuron-methyl on andisols and ultisols volcanic ash-derived soils: kinetics parameters and solute transport mechanisms. J Hazard Mater 2010;179:795–803.

[143] Nkedi-Kizza P, Shinde D, Savabi MR, Ouyang Y, Nieves L. Sorption kinetics and equilibria of organic pesticides in carbonatic soils from South Florida. J Environ Qual 2006;35:268–76.

[144] Yang X-Y, Al-Duri B. Application of branched pore diffusion model in the adsorption of reactive dyes on activated carbon. Chem Eng J 2001;83:15–23.

[145] Dzombak DA, Morel FMM. Sorption of cadmium on hydrous ferric oxide at high sorbate/sorbent ratios: equilibrium, kinetics, and modeling. J Colloid Interface Sci 1986;112:588–98.

[146] Marczewski AW. Application of mixed order rate equations to adsorption of methylene blue on mesoporous carbons. Appl Surf Sci 2010;256:5145–52.

[147] Liu Y, Shen L. From Langmuir kinetics to first- and second-order rate equations for adsorption. Langmuir 2008;24:11625–30.

[148] Han R, Wang Y, Zou W, Wang Y, Shi J. Comparison of linear and nonlinear analysis in estimating the Thomas model parameters for methylene blue adsorption onto natural zeolite in fixed-bed column. J Hazard Mater 2007;145:331–5.

[149] Bates DM, Watts DG. Nonlinear regression analysis and its applications. New York: Wiley; 1988.

[150] Kumar KV. Linear and non-linear regression analysis for the sorption kinetics of methylene blue onto activated carbon. J Hazard Mater 2006;137:1538–44.

[151] Ho Y-S. Selection of optimum sorption isotherm, 42. Carbon; 2004. p. 2115–16.

[152] Kinniburgh DG. General purpose adsorption isotherms. Environ Sci Technol 1986;20:895–904.

[153] Namasivayam C, Sangeetha D. Application of coconut coir pith for the removal of sulfate and other anions from water. Desalination 2008;219:1–13.

[154] Nouri L, Ghodbane I, Hamdaoui O, Chiha M. Batch sorption dynamics and equilibrium for the removal of cadmium ions from aqueous phase using wheat bran. J Hazard Mater 2007;149:115–25.

[155] Czinkota I, Földényi R, Lengyel Z, Marton A. Adsorption of propisochlor on soils and soil components equation for multi-step isotherms. Chemosphere 2002;48:725–31.

[156] Ungarish M, Aharoni C. Kinetics of chemisorption. Deducing kinetic laws from experimental data. J Chem Soc, Faraday Trans I 1981;77:975–85.

[157] Montgomery DC, Peck EA, Vining GG. Introduction to linear regression analysis, Hoboken, NJ: Wiley; 2012. 5th ed.

[158] Khanday WA, Marrakchi F, Asif M, Hameed BH. Mesoporous zeolite–activated carbon composite from oil palm ash as an effective adsorbent for methylene blue. J Taiwan Inst Chem Eng 2017;70:32–41.

[159] Kumar KV, Porkodi K, Rocha F. Isotherms and thermodynamics by linear and non-linear regression analysis for the sorption of methylene blue onto activated carbon: comparison of various error functions. J Hazard Mater 2008;151:794–804.

[160] Box GEP, Hunter WG, Hunter JS. Statistics for experimenters: an introduction to design, data analysis, and model building. New York: Wiley; 1978.

[161] Lazaridis NK, Asouhidou DD. Kinetics of sorptive removal of chromium(VI) from aqueous solutions by calcined Mg–Al–CO$_3$ hydrotalcite. Water Res 2003;37:2875–82.

[162] Lin CC, Lai YT. Adsorption and recovery of lead(II) from aqueous solutions by immobilized Pseudomonas Aeruginosa PU21 beads. J Hazard Mater 2006;137:99–105.

[163] Mangaleshwaran L, Thirulogachandar A, Rajasekar V, Muthukumaran C, Rasappan K. Batch and fixed bed column studies on nickel (II) adsorption from aqueous solution by treated polyurethane foam. J Taiwan Inst Chem Eng 2015;55:112–18.

[164] Pandey PK, Sharma SK, Sambi SS. Removal of lead(II) from waste water on zeolite-NaX. J Environ Chem Eng 2015;3:2604–10.

[165] Kul AR, Koyuncu H. Adsorption of Pb(II) ions from aqueous solution by native and activated bentonite: kinetic, equilibrium and thermodynamic study. J Hazard Mater 2010;179:332–9.

[166] Li G, Zhao Z, Liu J, Jiang G. Effective heavy metal removal from aqueous systems by thiol functionalized magnetic mesoporous silica. J Hazard Mater 2011;192:277–83.

[167] Rasouli M, Yaghobi N, Hafezi M, Rasouli M. Adsorption of divalent lead ions from aqueous solution using low silica nano-zeolite X. J Ind Eng Chem 2012;18:1970–6.

[168] W-j Shan, D-W Fang, Shuang Y, et al. Equilibrium, kinetics, and thermodynamics studies on the recovery of rhenium(VII) and molybdenum(VI) from industrial wastewater by chemically modified waste paper gel. J Chem Eng Data 2012;57:290–7.

[169] Shafique U, Ijaz A, Salman M, Wu Zaman, Jamil N, Rehman R, et al. Removal of arsenic from water using pine leaves. J Taiwan Inst Chem Eng 2012;43:256–63.

[170] Galindo LSG, AFd Almeida Neto, MGCd Silva, Vieira MGA. Removal of cadmium(II) and lead(II) ions from aqueous phase on sodic bentonite. Mater Res 2013;16:515–27.

[171] Khoramzadeh E, Nasernejad B, Halladj R. Mercury biosorption from aqueous solutions by Sugarcane Bagasse. J Taiwan Inst Chem Eng 2013;44:266–9.

[172] Ismaiel AA, Aroua MK, Yusoff R. Palm shell activated carbon impregnated with task-specific ionic-liquids as a novel adsorbent for the removal of mercury from contaminated water. Chem Eng J 2013;225:306–14.

[173] Fan H-T, Liu J-X, Yao H, Zhang Z-G, Yan F, W-X Li. Ionic imprinted silica–supported hybrid sorbent with an anchored chelating Schiff base for selective removal of cadmium(II) Ions from aqueous media. Ind Eng Chem Res 2014;53:369–78.

[174] Wan S, Ma Z, Xue Y, Ma M, Xu S, Qian L, et al. Sorption of lead(II), cadmium(II), and copper(II) ions from aqueous solutions using tea waste. Ind Eng Chem Res 2014;53:3629–35.

[175] Vincent T, Taulemesse JM, Dauvergne A, Chanut T, Testa F, Guibal E. Thallium(I) sorption using Prussian blue immobilized in alginate capsules. Carbohydr Polym 2014;99:517–26.

[176] Ghasemi M, Naushad M, Ghasemi N, Khosravi-fard Y. Adsorption of Pb(II) from aqueous solution using new adsorbents prepared from agricultural waste: adsorption isotherm and kinetic studies. J Ind Eng Chem 2014;20:2193–9.

[177] Fu R, Liu Y, Lou Z, Wang Z, Baig SA, Xu X. Adsorptive removal of Pb(II) by magnetic activated carbon incorporated with amino groups from aqueous solutions. J Taiwan Inst Chem Eng 2016;62:247–58.

[178] Igberase E, Osifo P. Equilibrium, kinetic, thermodynamic and desorption studies of cadmium and lead by polyaniline grafted cross-linked chitosan beads from aqueous solution. J Ind Eng Chem 2015;26:340–7.

[179] Zheng L, Meng P. Preparation, characterization of corn stalk xanthates and its feasibility for Cd (II) removal from aqueous solution. J Taiwan Inst Chem Eng 2016;58:391–400.

[180] Luo X, Ding L, Luo J. Adsorptive removal of Pb(II) ions from aqueous samples with amino-functionalization of metal–organic frameworks MIL-101(Cr). J Chem Eng Data 2015;60:1732–43.

[181] Tran L, Wu P, Zhu Y, Liu S, Zhu N. Comparative study of Hg(II) adsorption by thiol- and hydroxyl-containing bifunctional montmorillonite and vermiculite. Appl Surf Sci 2015;356:91–101.

[182] Ma L, Wang Q, Islam SM, Liu Y, Ma S, Kanatzidis MG. Highly selective and efficient removal of heavy metals by layered double hydroxide intercalated with the MoS₄²⁻ ion. J Am Chem Soc 2016;138:2858–66.

[183] Jalil AA, Triwahyono S, Yaakob MR, et al. Utilization of bivalve shell-treated Zea mays L. (maize) husk leaf as a low-cost biosorbent for enhanced adsorption of malachite green. Bioresour Technol 2012;120:218–24.

[184] Sapawe N, Jalil AA, Triwahyono S, et al. Cost-effective microwave rapid synthesis of zeolite NaA for removal of methylene blue. Chem Eng J 2013;229:388–98.

[185] Hameed BH, El-Khaiary MI. Sorption kinetics and isotherm studies of a cationic dye using agricultural waste: broad bean peels. J Hazard Mater 2008;154:639–48.

[186] Yılmaz E, Sert E, Atalay FS. Synthesis, characterization of a metal organic framework: MIL-53 (Fe) and adsorption mechanisms of methyl red onto MIL-53 (Fe). J Taiwan Inst Chem Eng 2016;65:323–30.

[187] Bhaumik M, McCrindle R, Maity A. Efficient removal of Congo red from aqueous solutions by adsorption onto interconnected polypyrrole–polyaniline nanofibres. Chem Eng J 2013;228:506–15.

[188] Slimani R, El Ouahabi I, Abidi F, et al. Calcined eggshells as a new biosorbent to remove basic dye from aqueous solutions: thermodynamics, kinetics, isotherms and error analysis. J Taiwan Inst Chem Eng 2014;45:1578–1587.

[189] Parshetti GK, Chowdhury S, Balasubramanian R. Hydrothermal conversion of urban food waste to chars for removal of textile dyes from contaminated waters. Bioresour Technol 2014;161:310–19.

[190] Kareem SH, Ali IH, Jalhoom MG. Synthesis and characterization of organic functionalized mesoporous silica and evaluate their adsorptive behavior for removal of methylene blue from aqueous solution. Am J Environ Sci 2014;10:48–60.

[191] Jin X, Yu B, Chen Z, Arocena JM, Thring RW. Adsorption of orange II dye in aqueous solution onto surfactant-coated zeolite: characterization, kinetic and thermodynamic studies. J Colloid Interface Sci 2014;435:15–20.

[192] El Haddad M. Removal of Basic Fuchsin dye from water using mussel shell biomass waste as an adsorbent: equilibrium, kinetics, and thermodynamics. J Taibah Univ Sci 2016;10:664–74.

[193] Zhao X, Liu S, Tang Z, et al. Synthesis of magnetic metal-organic framework (MOF) for efficient removal of organic dyes from water. Sci Rep 2015;5:11849.

[194] Liu L, Zhang B, Zhang Y, He Y, Huang L, Tan S, et al. Simultaneous removal of cationic and anionic dyes from environmental water using montmorillonite-pillared graphene oxide. J Chem Eng Data 2015;60:1270–8.

[195] Gao Y, Xu S, Yue Q, Wu Y, Gao B. Chemical preparation of crab shell-based activated carbon with superior adsorption performance for dye removal from wastewater. J Taiwan Inst Chem Eng 2016;61:327–35.

[196] Ghasemi M, Mashhadi S, Asif M, Tyagi I, Agarwal S, Gupta VK. Microwave-assisted synthesis of tetraethylenepentamine functionalized activated carbon with high adsorption capacity for Malachite green dye. J Mol Liq 2016;213:317–25.

[197] Saleh TA, Muhammad AM, Ali SA. Synthesis of hydrophobic cross-linked polyzwitterionic acid for simultaneous sorption of Eriochrome black T and chromium ions from binary hazardous waters. J Colloid Interface Sci 2016;468:324–33.

[198] Maneerung T, Liew J, Dai Y, Kawi S, Chong C, Wang CH. Activated carbon derived from carbon residue from biomass gasification and its application for dye adsorption: kinetics, isotherms and thermodynamic studies. Bioresour Technol 2016;200:350–9.

[199] Mohanty K, Das D, Biswas MN. Treatment of phenolic wastewater in a novel multi-stage external loop airlift reactor using activated carbon. Sep Purif Technol 2008;58:311–19.

[200] Nourmoradi H, Avazpour M, Ghasemian N, et al. Surfactant modified montmorillonite as a low cost adsorbent for 4-chlorophenol: equilibrium, kinetic and thermodynamic study. J Taiwan Inst Chem Eng 2016;59:244–51.

[201] Tseng RL, Wu KT, Wu FC, Juang RS. Kinetic studies on the adsorption of phenol, 4-chlorophenol, and 2,4-dichlorophenol from water using activated carbons. J Environ Manage 2010;91:2208–14.

[202] Ofomaja AE, Unuabonah EI. Kinetics and time-dependent Langmuir modeling of 4-nitrophenol adsorption onto Mansonia sawdust. J Taiwan Inst Chem Eng 2013;44:566–76.

[203] Huang J, Jin X, Deng S. Phenol adsorption on an N-methylacetamide–modified hypercrosslinked resin from aqueous solutions. Chem Eng J 2012;192:192–200.

[204] Pigatto G, Lodi A, Finocchio E, Palma MSA, Converti A. Chitin as biosorbent for phenol removal from aqueous solution: equilibrium, kinetic and thermodynamic studies. Chem Eng Process 2013;70:131–9.

[205] Cheng WP, Gao W, Cui X, Ma JH, Li RF. Phenol adsorption equilibrium and kinetics on zeolite X/activated carbon composite. J Taiwan Inst Chem Eng 2016;62:192–8.

[206] Park Y, Sun Z, Ayoko GA, Frost RL. Bisphenol A sorption by organo-montmorillonite: implications for the removal of organic contaminants from water. Chemosphere 2014;107:249–56.

[207] Huang L, Zhou Y, Guo X, Chen Z. Simultaneous removal of 2,4-dichlorophenol and Pb(II) from aqueous solution using organoclays: isotherm, kinetics and mechanism. J Ind Eng Chem 2015;22:280–7.

[208] Abdel-Ghani NT, El-Chaghaby GA, Helal FS. Individual and competitive adsorption of phenol and nickel onto multiwalled carbon nanotubes. J Adv Res 2015;6:405–15.

[209] Peng S, Hao K, Han F, et al. Enhanced removal of bisphenol-AF onto chitosan–modified zeolite by sodium cholate in aqueous solutions. Carbohydr Polym 2015;130:364–71.

[210] Sadasivam S, Krishna SK, Ponnusamy K, Nagarajan GS, Kang TW, Venkatesalu SC. Equilibrium and thermodynamic studies on the adsorption of an organophosphorous pesticide onto "waste" jute fiber carbon. J Chem Eng Data 2010;55:5658–62.

[211] Njoku VO, Foo KY, Hameed BH. Microwave-assisted preparation of pumpkin seed hull activated carbon and its application for the adsorptive removal of 2,4-dichlorophenoxyacetic acid. Chem Eng J 2013;215-216:383–8.

[212] Caceres-Jensen L, Rodriguez-Becerra J, Parra-Rivero J, Escudey M, Barrientos L, Castro-Castillo V. Sorption kinetics of diuron on volcanic ash derived soils. J Hazard Mater 2013;261:602–13.

[213] Ganiyu SO, Bispo C, Bion N, Ferreira P, Batonneau-Gener I. Periodic mesoporous organosilicas as adsorbents for the organic pollutants removal in aqueous phase. Microporous Mesoporous Mater 2014;200:117–23.

[214] Kuśmierek K, Szala M, Świątkowski A. Adsorption of 2,4-dichlorophenol and 2,4-dichlorophenoxyacetic acid from aqueous solutions on carbonaceous materials obtained by combustion synthesis. J Taiwan Inst Chem Eng 2016;63:371–8.

[215] Gu Z, Gao M, Lu L, Liu Y, Yang S. Montmorillonite functionalized with zwitterionic surfactant as a highly efficient adsorbent for herbicides. Ind Eng Chem Res 2015;54:4947–55.

[216] Zhu X, Li B, Yang J, Li Y, Zhao W, Shi J, et al. Effective adsorption and enhanced removal of organophosphorus pesticides from aqueous solution by Zr-based MOFs of UiO-67. ACS Appl Mater Interfaces 2015;7:223–31.

[217] Tang L, Zhang S, Zeng GM, et al. Rapid adsorption of 2,4-dichlorophenoxyacetic acid by iron oxide nanoparticles-doped carboxylic ordered mesoporous carbon. J Colloid Interface Sci 2015;445:1–8.

[218] Ouali A, Belaroui LS, Bengueddach A, Galindo AL, Peña A. Fe₂O₃–palygorskite nanoparticles, efficient adsorbates for pesticide removal. Appl Clay Sci 2015;116:67–75.

[219] Rasamimanana S, Mignard S, Batonneau-Gener I. Hierarchical zeolites as adsorbents for mesosulfuron-methyl removal in aqueous phase. Microporous Mesoporous Mater 2016;226:153–61.

[220] Cobas M, Meijide J, Sanromán MA, Pazos M. Chestnut shells to mitigate pesticide contamination. J Taiwan Inst Chem Eng 2016;61:166–73.

[221] Calisto V, Ferreira CI, Oliveira JA, Otero M, Esteves VI. Adsorptive removal of pharmaceuticals from water by commercial and waste-based carbons. J Environ Manag 2015;152:83–90.

[222] Mendez-Diaz JD, Prados-Joya G, Rivera-Utrilla J, Leyva-Ramos R, Sanchez-Polo M, Ferro-Garcia MA, et al. Kinetic study of the adsorption of nitroimidazole antibiotics on activated carbons in aqueous phase. J Colloid Interface Sci 2010;345:481–90.

[223] Erdinc N, Gokturk S, Tuncay M. A study on the adsorption characteristics of an amphiphilic phenothiazine drug on activated charcoal in the presence of surfactants. Colloids Surf B: Biointerfaces 2010;75:194–203.

[224] Li Z, Chang PH, Jiang WT, Jean JS, Hong H, Liao L. Removal of diphenhydramine from water by swelling clay minerals. J Colloid Interface Sci 2011;360:227–32.

[225] Hu D, Wang L. Adsorption of amoxicillin onto quaternized cellulose from flax noil: kinetic, equilibrium and thermodynamic study. J Taiwan Inst Chem Eng 2016;64:227–34.

[226] Ahmed MJ, Theydan SK. Fluoroquinolones antibiotics adsorption onto microporous activated carbon from lignocellulosic biomass by microwave pyrolysis. J Taiwan Inst Chem Eng 2014;45:219–26.

[227] Reza RA, Ahmaruzzaman M, Sil AK, Gupta VK. Comparative adsorption behavior of ibuprofen and clofibric acid onto microwave assisted activated bamboo waste. Ind Eng Chem Res 2014;53:9331–9.

[228] Fakhri A, Adami S. Adsorption and thermodynamic study of Cephalosporins antibiotics from aqueous solution onto MgO nanoparticles. J Taiwan Inst Chem Eng 2014;45:1001–6.

[229] Li JR, Wang YX, Wang X, Yuan B, Fu ML. Intercalation and adsorption of ciprofloxacin by layered chalcogenides and kinetics study. J Colloid Interface Sci 2015;453:69–78.

[230] Qin L, Zhou Z, Dai J, et al. Novel N-doped hierarchically porous carbons derived from sustainable shrimp shell for high-performance removal of sulfamethazine and chloramphenicol. J Taiwan Inst Chem Eng 2016;62:228–38.

[231] Zhang D, Yin J, Zhao J, Zhu H, Wang C. Adsorption and removal of tetracycline from water by petroleum coke-derived highly porous activated carbon. J Environ Chem Eng 2015;3:1504–12.

[232] Kyzas GZ, Deliyanni EA. Modified activated carbons from potato peels as green environmental-friendly adsorbents for the treatment of pharmaceutical effluents. Chem Eng Res Des 2015;97:135–44.

[233] Álvarez-Torrellas S, Rodríguez A, Ovejero G, García J. Comparative adsorption performance of ibuprofen and tetracycline from aqueous solution by carbonaceous materials. Chem Eng J 2016;283:936–47.

[234] Liu B, Peng X, Chen W, Li Y, Meng X, Wang D, et al. Adsorptive removal of patulin from aqueous solution using thiourea modified chitosan resin. Int J Biol Macromol 2015;80:520–8.

[235] Gusmao KA, Gurgel LV, Melo TM, Carvalho Cde F, Gil LF. Adsorption studies of etherdiamine onto modified sugarcane bagasses in aqueous solution. J Environ Manag 2014;133:332–42.

[236] da Silva CM, Rocha Qda C, Rocha PC, Louvisse AM, Lucas EF. Removal of naphthalene from aqueous systems by poly(divinylbenzene) and poly(methyl methacrylate-divinylbenzene) resins. J Environ Manag 2015;157:205–12.

[237] Xu C, Chen H, Jiang F. Adsorption of perflourooctane sulfonate (PFOS) and perfluorooctanoate (PFOA) on polyaniline nanotubes. Colloids Surf A: Physicochem Eng Aspects 2015;479:60–7.

[238] Heibati B, Ghoochani M, Albadarin AB, et al. Removal of linear alkyl benzene sulfonate from aqueous solutions by functionalized multi-walled carbon nanotubes. J Mol Liq 2016;213:339–44.

[239] Eckenfelder Jr WW. Industrial Water Pollution Control. McGraw hill publication. USA; 1989.

[240] Noll KE, Gounaris V, Hou W-s. Adsorption technology for air and water pollution control. Chelsea, Mich: Lewis Publishers; 1992.

[241] Plaza MG, García S, Rubiera F, Pis JJ, Pevida C. Post-combustion CO_2 capture with a commercial activated carbon: comparison of different regeneration strategies. Chem Eng J 2010;163:41–7.

[242] Farooq S, Qinglin H, Karimi IA. Identification of transport mechanism in adsorbent micropores from column dynamics. Ind Eng Chem Res 2002;41:1098–106.

[243] Casas N, Schell J, Pini R, Mazzotti M. Fixed bed adsorption of CO_2/H_2 mixtures on activated carbon: experiments and modeling. Adsorption 2012;18:143–61.

[244] Thomas HC. Heterogeneous ion exchange in a flowing system. J Am Chem Soc 1944;66:1664–6.

[245] Najafi Nobar S, Farooq S. Experimental and modeling study of adsorption and diffusion of gases in Cu-BTC. Chem Eng Sci 2012;84:801–13.

[246] Chu KH. Improved fixed bed models for metal biosorption. Chem Eng J 2004;97:233–9.

[247] Bohart GS, Adams EQ. Some aspects of the behavior of charcoal with respect to chlorine. J Am Chem Soc 1920;42:523–44.

[248] Chu KH. Fixed bed sorption: setting the record straight on the Bohart–Adams and Thomas models. J Hazard Mater 2010;177:1006–12.

[249] Yoon YH, Nelson JH. Application of gas adsorption kinetics I. A theoretical model for respirator cartridge service life. Am Ind Hyg Assoc J 1984;45:509–516.

[250] Rao KS, Anand S, Venkateswarlu P. Modeling the kinetics of Cd(II) adsorption on Syzygium cumini L leaf powder in a fixed bed mini column. J Ind Eng Chem 2011;17:174–81.

[251] Cabrera-Lafaurie WA, Roman FR, Hernandez-Maldonado AJ. Single and multi-component adsorption of salicylic acid, clofibric acid, carbamazepine and caffeine from water onto transition metal modified and partially calcined inorganic–organic pillared clay fixed beds. J Hazard Mater 2015;282:174–82.

[252] Chatterjee A, Schiewer S. Biosorption of cadmium(II) ions by citrus peels in a packed bed column: effect of process parameters and comparison of different breakthrough curve models. Clean - Soil Air Water 2011;39:874–81.

[253] Hutchins R. New method simplifies design of activated-carbon systems. Am J Chem Eng 1973;80:133–8.

[254] Clark RM. Evaluating the cost and performance of field-scale granular activated carbon systems. Environ Sci Technol 1987;21:573–80.

[255] Medvidović NV, Perić J, Trgo M. Testing of breakthrough curves for removal of lead ions from aqueous solutions by natural zeolite-clinoptilolite according to the clark kinetic equation. Sep Sci Technol 2008;43:944–59.

[256] Wolborska A. Adsorption on activated carbon of p-nitrophenol from aqueous solution. Water Res 1989;23:85–91.

[257] Dulman V, Cucu-Man S-M, Bunia I, Dumitras M. Batch and fixed bed column studies on removal of Orange G acid dye by a weak base functionalized polymer. Desalin Water Treat 2015;57:14708–27.

[258] Singh N, Balomajumder C. Continuous packed bed adsorption of phenol and cyanide onto modified rice husk: an experimental and modeling study. Desalin Water Treat 2016;1–15.

[259] Hamdaoui O. Removal of copper(II) from aqueous phase by Purolite C100-MB cation exchange resin in fixed bed columns: modeling. J Hazard Mater 2009;161:737–46.

[260] Djelloul C, Hamdaoui O. Dynamic adsorption of methylene blue by melon peel in fixed-bed columns. Desalin Water Treat 2014;1–10.

[261] Yan G, Viraraghavan T, Chen M. A new model for heavy metal removal in a biosorption column. Adsorpt Sci Technol 2001;19:25–43.

[262] Zeinali F, Ghoreyshi AA, Najafpour G. Removal of toluene and dichloromethane from aqueous phase by granular activated carbon (GAC). Chem Eng Commun 2012;199:203–20.

[263] Singh A, Kumar D, Gaur JP. Continuous metal removal from solution and industrial effluents using Spirogyra biomass-packed column reactor. Water Res 2012;46:779–88.

[264] Ahmad AA, Idris A, Hameed BH. Color and COD reduction from cotton textile processing wastewater by activated carbon derived from solid waste in column mode. Desalin Water Treat 2012;41:224–31.

[265] Yagub MT, Sen TK, Afroze S, Ang HM. Fixed-bed dynamic column adsorption study of methylene blue (MB) onto pine cone. Desalin Water Treat 2014;55:1026–39.

[266] Sotelo JL, Ovejero G, Rodríguez A, Álvarez S, García J. Removal of atenolol and isoproturon in aqueous solutions by adsorption in a fixed-bed column. Ind Eng Chem Res 2012;51:5045–55.

[267] Sotelo JL, Rodríguez A, Álvarez S, García J. Removal of caffeine and diclofenac on activated carbon in fixed bed column. Chem Eng Res Des 2012;90:967–74.

[268] Wu Y, Wang Y, Wang J, Xu S, Yu L, Philippe C, et al. Nitrate removal from water by new polymeric adsorbent modified with amino and quaternary ammonium groups: batch and column adsorption study. J Taiwan Inst Chem Eng 2016;66:191–9.

[269] Tchobanoglous G, Burton FL. Wastewater engineering: treatment, disposal and reuse, 3rd edition. McGraw-Hill; 1991. p. 321.